WADC TECHNICAL REPORT 57-351
ASTIA DOCUMENT NO. AD 130790

THE INFLUENCE OF GEOMETRY PARAMETERS UPON LAG ERROR IN AIRBORNE PRESSURE MEASURING SYSTEMS

J. P. LAMB JR., 1st Lt, USAF

FLIGHT CONTROL LABORATORY

JULY 1957

WRIGHT AIR DEVELOPMENT CENTER

AF-WP-(B)-O-27 JUL 57 125

WADC TECHNICAL REPORT 57-351

THE INFLUENCE OF GEOMETRY PARAMETERS UPON LAG ERROR IN AIRBORNE PRESSURE MEASURING SYSTEMS

J. P. Lamb Jr., 1st Lt, USAF

Flight Control Laboratory

July 1957

Project No. 913A

Wright Air Development Center
Air Research and Development Command
United States Air Force
Wright-Patterson Air Force Base, Ohio

FOREWORD

The investigation reported herein was conducted by the author while in the Instruments Branch of the Flight Control Laboratory at the Wright Air Development Center. The experimental phase of the study was accomplished at the Inland Testing Laboratories in Dayton, Ohio.

The author wishes to acknowledge the cooperation of the following persons: Mr. R. L. Fine, who first suggested the investigation and later contributed much constructive criticism; Messrs. F. S. Carothers and D. C. Wujciak, who provided valuable assistance in the testing program.

ABSTRACT

The general nature of the lag problem in airborne pressure measuring systems is discussed. It is concluded that variations in system geometry offer the most promise in improving response. The remainder of the report is given to a theoretical examination of various geometry parameters and to an evaluation (utilizing both theoretical and experimental methods) of their effect upon lag error. Techniques for computing lag error in any system are presented. Theory and experiment are shown to be in agreement for the case of laminar flow. Evidence of transitional flow is also presented. Based upon the results of the study, specific dimensions for tubing lines and pitot-static tube chambers are recommended for use in the static pressure systems of high performance aircraft.

PUBLICATION REVIEW

The publication of this report does not constitute approval by the Air Force of the findings or conclusions contained herein. It is published only for the exchange and stimulation of ideas.

FOR THE COMMANDER:

for C. R. Bryan

JOHN L. MARTIN, JR.
Colonel, USAF
Chief, Flight Control Laboratory

TABLE OF CONTENTS

LIST OF FIGURES

LIST OF TABLES

LIST OF SYMBOLS

A	Cross-sectional area
a	Speed of pressure propagation inside small ID tubing
D	Diameter
g	Gravitational constant
H	Pressure altitude
ln	Natural logarithm
ℓ	Length
n	Polytropic exponent
P	Pressure
ρ	Density
Re	Reynolds number
r	Radius
T	Absolute temperature
μ	Coefficient of viscosity
V	Volume
v	Velocity

Subscripts

f	Frictional
eq	Equivalent circular
cr	Critical

SECTION I

INTRODUCTION

The operational characteristics of high performance air vehicles require precise determination of various flight control parameters, some of which are not directly measureable but must be computed from measurements of basic variables of the immediate atmospheric environment. Two of the more important fundamental quantities which require measurement are total and static pressure. Accurate sensing of these pressures is necessary to assure the fidelity of such control parameters as Mach number, pressure altitude, airspeed, vertical speed, and air density.

The total inaccuracy of an airborne pressure measuring system is commonly separated into instrument errors and installation errors. The latter class of errors may be categorized as follows:

(1) Error associated with the geometry of the pressure sensing device.
(2) Error induced by the field of flow about the vehicle.
(3) Error resulting from a pressure lag in the tubing which connects the instruments with the sensor.

The scope of the present report will be limited to the last of the above sources of inaccuracy.

Basically, lag error occurs in the following manner: When the local pressure at the sensing device is changing (as, for example, in a climb, dive, or acceleration) air must flow to or from the instruments through the connecting tubing in order to maintain pressure equilibrium. While this air flow is in progress, a pressure drop exists between the ends of the tubing, resulting in a pressure lag at the instruments. Lag error is thus a dynamic characteristic and hence, has a direct effect upon system response.

Recent increases in aircraft performance have magnified the response problem considerably. Pressure system designs which were satisfactory in the past have proven to be inadequate (from a response standpoint) for use on high performance vehicles. As an initial step in alleviating this condition, an investigation of parameters affecting lag error was made at the Wright Air Development Center. The major objective of this study was to determine the most practical method for improving system response. Further, it was deemed desirable to present analytical procedures for predicting the pressure lag of any system for certain input conditions. Such procedures would enable designers to compare the lag characteristics of various proposed systems, thereby providing criteria for the selection of the most promising systems. In this way time consuming and costly experimental comparison could be minimized since only one (or possibly two) systems would require any laboratory investigation.

Manuscript released by the author 1 July 1957 for publication as a WADC Technical Report.

SECTION II

GENERAL NATURE OF THE PROBLEM

Before commencing a detailed examination of the mechanics of pressure lag, it is well to discuss the qualitative aspects and general nature of the problem.

The total lag of a system may be conveniently expressed as a sum of two components; acoustic lag and flow lag. The acoustic lag is associated with the finite time required for a pressure change to be propagated from the system inlet to the point for which the lag is desired. The flow lag, on the other hand, is a consequence of the fluid velocity in the tubing and may itself be subdivided into (1) the lag due to frictional resistance and (2) the lag resulting from fluid inertia. In general, the largest of the three lag effects is that due to friction (or the viscous lag). The acoustic lag is usually next in magnitude while inertia effects are negligible in most cases since both the air mass and the fluid velocity are relatively small.

Almost any parameter which directly affects lag error in an airborne system is associated with one or more of the following sources of influence.

(1) Forcing functions
(2) Thermodynamic characteristics
(3) Geometry factors

Some idea of the general complexity of the lag problem may be gained through a brief examination of the nature of these influencing parameters.

Forcing Functions - Since forcing functions are directly related to aircraft maneuvers, it is obvious that an airborne system may be acted upon by an unlimited number of pressure-time input functions. Three common types of inputs to a static pressure system are illustrated in Figure 1.

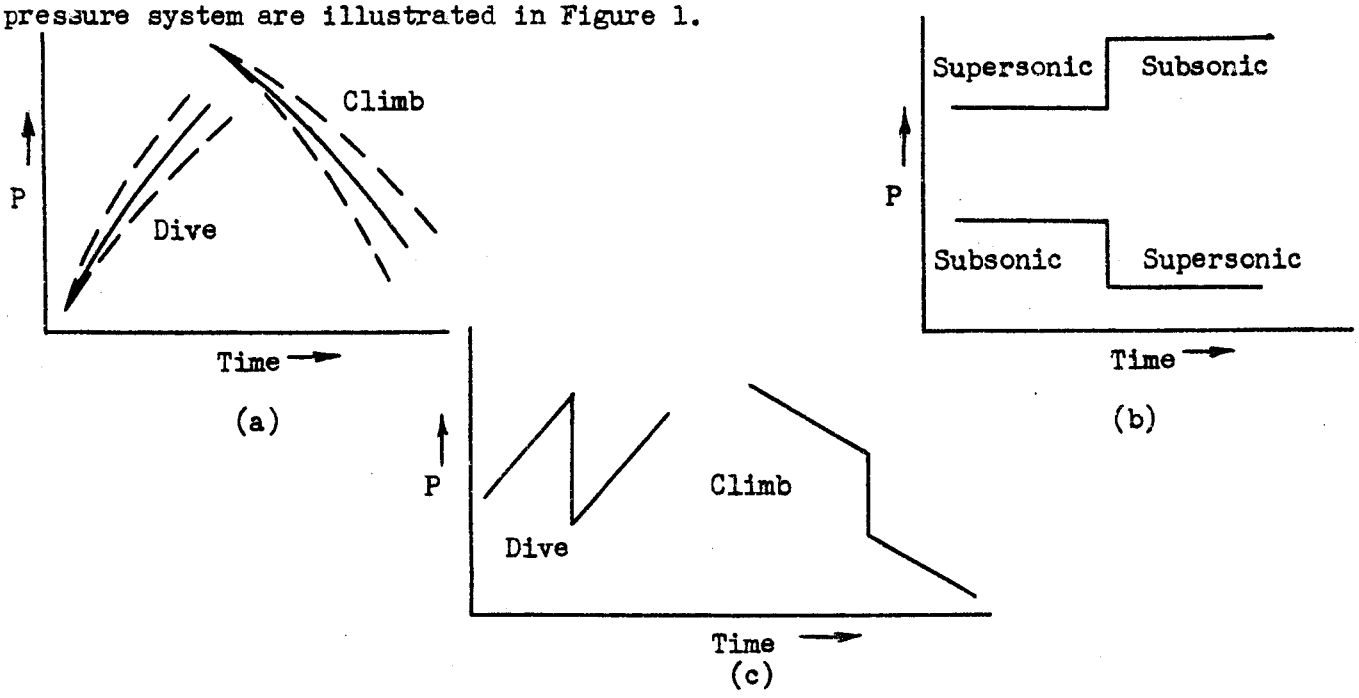

Figure 1 Typical Static Pressure System Inputs

The inputs of Figure 1(a) would exist if an aircraft were maintaining a constant vertical speed. Consider also an aircraft passing through the sonic region in level flight. As the fuselage bow wave moves to the vicinity of the static pressure ports, the step function inputs of Figure 1(b) will act upon the system. In the case where the vehicle climbs or dives through the sonic barrier the curves of Figure 1(c) apply. The wide range of possible input shapes is readily evident.

The forcing function is of major importance since its characteristics determine the type of the flow (laminar, transitional, or turbulent) within the system. This, of course, implies the existence of a certain level of friction. The magnitude of the input (or forcing) pressure is also important. For instance, in a total pressure system a given pressure drop might be insignificant whereas in a static pressure system the same pressure drop could constitute a large error. For this reason the present report, though applicable to any airborne system, will emphasize lag problems in static pressure systems.

Thermodynamic Characteristics - The frictional and damping qualities of the air within the system are influenced largely by the viscosity which, in turn, is a function of the air temperature. This parameter is determined by the amount of heat transfered to the air from (1) the interior of the aircraft through the metal tubing walls and (2) any incoming air which may be at a different temperature from the air already within the system. The air temperature also affects the acoustic lag since the speed of pressure propagation is a direct function of the temperature.

Geometry Factors - This group of parameters includes the physical dimensions of the system, i.e., such factors as length and diameter of tubing lines, internal volumes, fittings, bends, and restrictions in the flow path. These factors, collectively, establish the over-all frictional level of a system for a given flow condition.

In light of the stated objective (that of determining the most practical method of response improvement), a conclusion of considerable importance may be drawn from the preceding paragraphs: Of these three groups of influencing parameters, only one group, the last, is subject to any significant manipulation by the designer. Emphasis, therefore, in the WADC investigation was given to (1) the examination of various geometry factors and (2) the evaluation of their effect upon lag error.

SECTION III

ANALYSIS

3.1 Literature Review

A number of analyses of pressure lag, employing various approaches, are available in the literature. One method, presented by Huston (ref. 5) makes use of a linear differential equation which describes the response of a resistance-capacitance electrical circuit. This equation is converted by analogy to a pressure expression in which the electrical resistance is a function of the fluid viscosity and the length and diameter of the system tubing, and the electrical capacity is represented by the internal pressure and volume of the instrument.

Some recent investigators (refs. 6,8, and 13), however, have analyzed the problem more rigorously through the use of basic fluid mechanics principles such as the Navier-Stokes equation and the equation of continuity. It is believed that analyses of this type lend themselves to a better over-all understanding of the problem than less rigorous approaches. The theoretical derivations herein are similar to those of Newman (ref. 8).

A variety of methods for experimental lag determination have been proposed and/or attempted. Two techniques, each involving a characteristic forcing function, have received considerable attention. One scheme, which was utilized by most early investigators, (ref. 15), concerns the application of a pressure step function. The resulting exponential response is then monitored and a lag (or time) constant determined therefrom. In the second case, a ramp function (or constant pressure rate) serves as the input. The advantage of the step input lies in its ease of production and application. The main disadvantage is that it introduces secondary effects, such as the damping, inertia, and Reynolds number effects into the response. These phenomena are variable and somewhat difficult to analyze. On the other hand, the ramp input, though harder to produce, results in a near constant rate of air flow within the system and, as such, can be correlated with analytical results fairly easily. Furthermore, the ramp function simulates rather closely a dive or climb.

It was originally believed that both of these test methods yielded identical results. Subsequent investigation (refs. 4 and 14), however, did not corroborate this supposition. These tests indicated that, when the step input was employed, the value of the lag constant was dependent upon the size of the applied pressure step. Head (ref. 4), among others, suggested that the lag constant be determined for a number of step sizes and the resulting data be extrapolated to zero step size.

Vaughn (ref. 14) reviewed the situation and concluded that the basic difficulty lay in the use of a linear differential equation. He later developed a non-linear theory based upon an empirical equation derived by Perry (ref. 9). This equation described the mass flow through a sharp-edged orifice in terms of the pressures on either side of the orifice and the absolute temperature upstream of the orifice. Though somewhat complicated, this theory appears to be capable of application over a large range of input functions. It could not, however, be easily adapted to the present investigation.

3.2 The Basic System

To treat the most generalized case of pressure lag - including the interaction of those influencing parameters discussed in Section II - would require an analysis of such rigor and complexity as to render it impractical. Hence, as in many other problems, it is necessary to resort to simplified approaches which lend themselves to analytical treatment but which, at the same time, furnish information of value concerning the real and more complicated situation.

A simple pressure measuring system consisting of a single length of uniform tubing connected to an instrument will now be examined. Such an arrangement is shown in Figure 2.

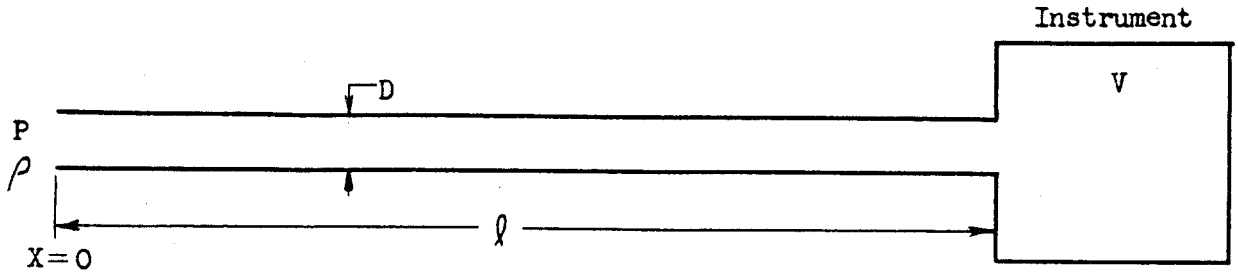

Figure 2 The Basic System

The following assumptions will be made in the analysis:

(1) incompressible fluid,
(2) one-dimensional, steady flow,
(3) laminar frictional values,
(4) isothermal fluid conditions, and
(5) ramp forcing function.

Three fundamental principles will serve as the basis for the development of an equation for the pressure drop due to friction in this system. They are:

(1) Navier-Stokes equation (equation of motion),
(2) Equation of state, and
(3) Equation of continuity.

For one-dimensional steady flow the Navier-Stokes equation becomes

$$\frac{r}{\mu}\frac{\partial P}{\partial X}=\frac{\partial}{\partial r}\left[r\frac{\partial v}{\partial r}\right] \qquad (1)$$

Applying laminar flow boundary conditions to this equation after integration produces the common Hagen-Poissueille law. (See Derivation Summary 1, Appendix I.)

$$\frac{dP}{dX}=-\frac{32\mu v}{D^2} \qquad (2)$$

The general polytropic equation of state for air is

$$\frac{P}{\rho^n} = \text{constant} \tag{3}$$

Differentiating with respect to time yields

$$\dot{P} = cn\rho^{n-1}\dot{\rho} \tag{4}$$

The value of "n" will vary between unity (for isothermal conditions) and 1.4 (for the adiabatic situation) depending upon the amount of heat transfered to the air within the system. Experimental ground tests by Newman (ref. 8) and flight test data presented by Vaughn (ref. 14) indicate very strongly that in most cases the actual flow is near isothermal. For such conditions, n=1 and equation (4) becomes

$$\dot{P} = c\dot{\rho} \tag{5}$$

Experimental data also show that, for a ramp input, the rate of pressure change is very nearly constant throughout the system. The conclusion, therefore, is that the rate of density change is also constant in the system.

The equation of continuity for one-dimensional, steady flow may be written as

$$\dot{\rho} + \frac{d}{dX}\left[\rho v\right] = 0 \tag{6}$$

with the boundary condition that, at $X = \ell$,

$$\left[\rho v\right]_\ell = \frac{V}{A}\left[\dot{\rho}\right]_\ell \tag{7}$$

Integrating equation (6) along the tubing length (remembering that $\dot{\rho}$ = constant) and substituting equation (7) yields

$$\rho v = \left[(\ell - X) + \frac{V}{A}\right]\dot{\rho}$$

Solving this expression for v and substituting it into equation (2) gives

$$\frac{dP}{dX} = -\frac{32\mu}{D^2}\left[(\ell - X) + \frac{V}{A}\right]\frac{\dot{\rho}}{\rho} \tag{8}$$

An integration of equation (8) results in an expression for the frictional pressure drop between the ends of the tubing. Thus

$$\Delta P_f = \frac{32\mu\ell}{AD^2}\left[V + \frac{A\ell}{2}\right]\frac{\dot{\rho}}{\rho} \tag{9}$$

It is desirable at this point to replace the density terms in equation (9)

with equivalent pressure functions. This may be done by considering again the equation of state (equation 3) with n=1. Then

$$P = C\rho$$
$$\dot{P} = C\dot{\rho}$$
and
$$\frac{\dot{P}}{P} = \frac{\dot{\rho}}{\rho} \tag{10}$$

The term $\frac{Al}{2}$ in equation (9) is one-half the tubing volume and may be denoted as $V_t/2$. Substituting equation (10) into (9) and making the notation change, yields the equation below.

$$\Delta P_f = \frac{128\mu l}{\pi D^4}\left[V + \frac{V_t}{2}\right]\frac{\dot{P}}{P} \tag{11}$$

Equation (11) is the fundamental viscous lag expression for the simple system under consideration. It is to be noted that the internal volume V of the instrument is theoretically a function of the pressure within the volume. In a total pressure system the volume might be that inside a diaphragm. In such a case the change in volume with pressure would be appreciable. However, in a static pressure system, V would probably be the internal volume of an instrument case and the change in volume would be much less significant.

The pressure drop given in equation (11) has been visualized in two ways by various investigators. In one instance, equation (11) is re-written as

$$\Delta P_f = \lambda \dot{P} \tag{12}$$

in which the term λ is the steady state viscous lag (or time) constant of the system. It can be seen from a comparison of equations (11) and (12) that

$$\lambda \propto \frac{\mu}{P} \tag{13}$$

It follows then that

$$\frac{\lambda}{\lambda_o} = \frac{\mu}{\mu_o}\frac{P_o}{P} \tag{14}$$

where the "o" subscripts refer to sea level standard conditions. In Figure 3 λ/λ_o is plotted against altitude for a standard atmosphere and for constant temperature conditions. It is readily apparent from this curve that the lag constant (and consequently the pressure drop or lag error) increases quite rapidly with altitude.

It is often convenient to convert equation (12) into altitude error. This may be accomplished when it is recalled that

$$\left.\begin{aligned}\frac{dP}{dH} &= -\rho g \\ \dot{P} &= -\rho g \dot{H}\end{aligned}\right\} \tag{15}$$

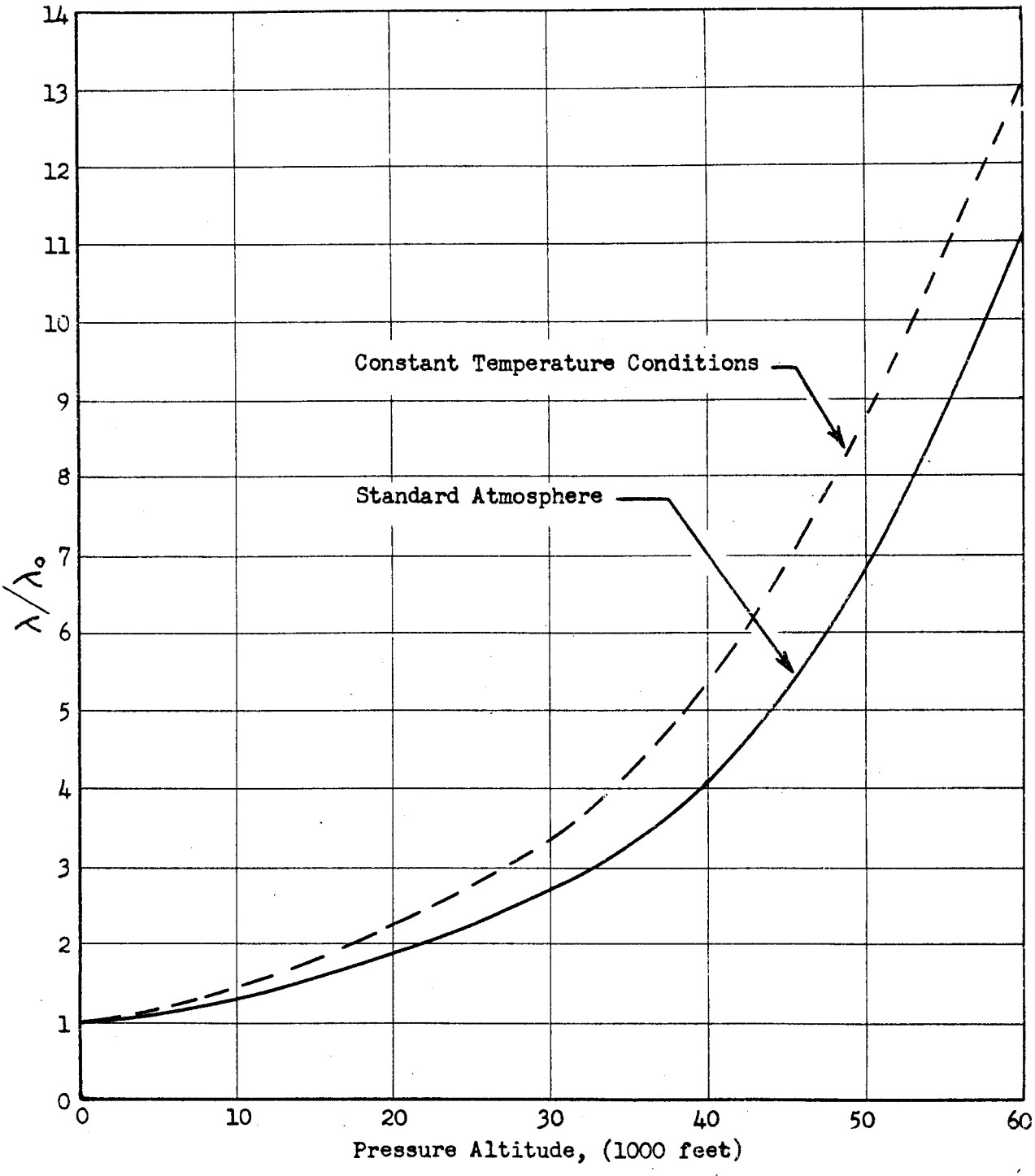

Figure 3 Variation of Viscous Lag Constant With Altitude

After substitution of equation (15) into equation (12), the latter expression becomes

$$\Delta H = \lambda \dot{H} \tag{16}$$

which relates the altitude error (equivalent to ΔP_f) and the vertical speed. Obviously, λ must be evaluated at the pressure or altitude at which the error is desired.

The second method of analyzing equation (11) involves the following equation:

$$\Delta P_f = \beta \frac{\dot{P}}{P} \tag{17}$$

where

$$\beta = \frac{128 \mu l}{\pi D^4} \left[V + \frac{V_t}{2} \right]$$

Newman (ref. 8) has found this form of equation (11) to be useful in studying ground lag tests. It is seen that, for the assumed isothermal, laminar flow conditions, β is constant for a given configuration. Thus, if the frictional pressure drop (ΔP_f) is plotted vs. $\dot{P}/P$, a straight line results. This procedure will be utilized in a subsequent article to present experimental data.

Thus far the development has dealt with the viscous lag. The corresponding acoustic lag expression is

$$\Delta P_a = \frac{l}{a} \dot{P} \tag{18}$$

The speed of pressure propagation inside small diameter tubing is normally considered to be approximately 1000 feet per second (or 12,000 in. per sec) at standard conditions. Assuming that "a" decreases as the square root of the absolute temperature, the equation for the acoustic velocity is then

$$a = 12{,}000 \sqrt{\frac{T}{T_o}} \tag{19}$$

where T_o = 288°K or 519°R.

3.3 More Complex Systems

Since the geometry of actual airborne installations is usually more complex than the simple arrangement previously discussed, equation (11) cannot be applied directly to such cases without some prior generalization. For instance, a typical static pressure system consists of a pitot-static tube connected to a main tubing line from which branches are led to the various instruments. In such a system it has been found necessary to consider each length of tubing separately.

Before analyzing an actual installation, however, it is desirable to further examine equation (11) which is repeated here for reference.

$$\Delta P_f = \frac{128 \mu \ell}{\pi D^4}\left[V + \frac{V_t}{2}\right]\frac{\dot{P}}{P} \qquad (11)$$

It is recalled that, in the preceding article, the term V represented the internal volume of the measuring instrument. In the more general case it may be assumed that V is the <u>total</u> volume (instruments and tubing) which is downstream (away from the source) from the length of tubing under consideration. Newman (ref. 8) has demonstrated the validity of this assumption in the following manner: Consider again the simple system shown below.

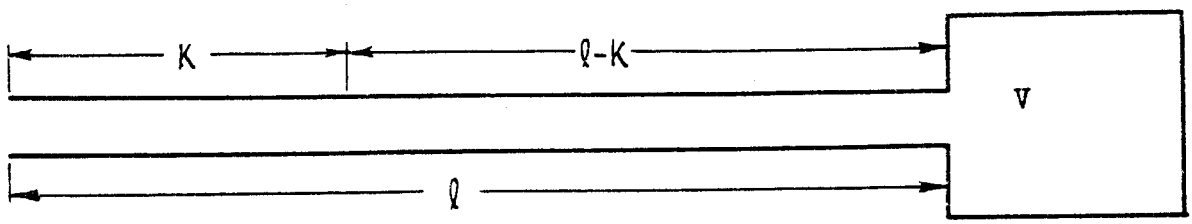

The tubing is divided into two arbitrary lengths. If the assumption holds then the total lag is equal to the sum of the lags of each arbitrary length, or

$$\Delta P_f\Big]_\ell = \Delta P_f\Big]_{\ell-K} + \Delta P_f\Big]_K \qquad (20)$$

If equation (11) is applied to each term of equation (20) and the resulting expression simplified (see Derivation Summary 2) it will be seen that the assumption is valid. Thus, with a slight change in symbolism, equation (11) may be written as

$$\Delta P_{f\ell} = \frac{128 \mu \ell}{\pi D^4}\left[V_d + \frac{V_\ell}{2}\right]\frac{\dot{P}}{P} \qquad (21)$$

The subscripts ℓ and d refer respectively to "length ℓ " and "downstream". The previous definitions of λ and β may also be correspondingly modified.

To demonstrate calculation technique, a typical arrangement, shown in Figure 4, will be examined.

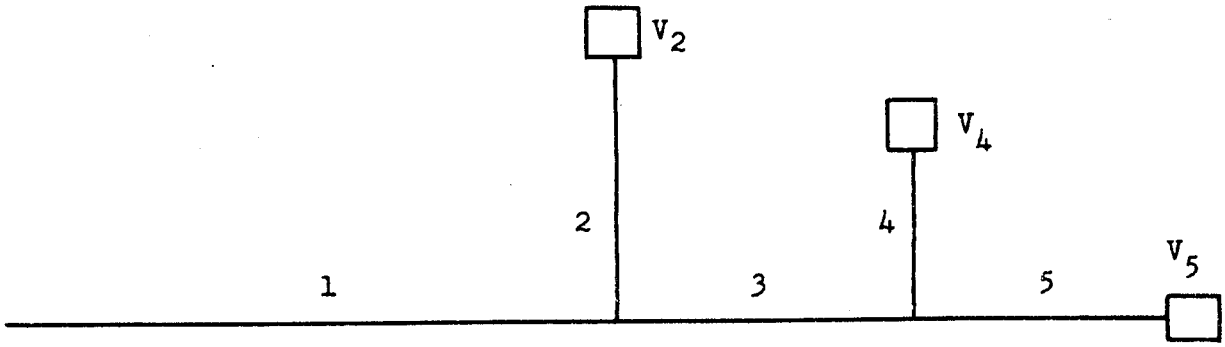

Figure 4 Typical Static Pressure System

Disregarding for the moment the pitot-static tube, the total lag (both acoustic and viscous) to each instrument volume may be found by the following procedure: First, λ_o or β_o is determined for each length of tubing. For a given tubing ID

$$\lambda_o = B\,\ell\left[V_d + \frac{A\ell}{2}\right]$$

and

$$\beta_o = C\,\ell\left[V_d + \frac{A\ell}{2}\right]$$

where

$$A = \frac{\pi}{4} D^2$$

$$B = \frac{128\,\mu_o}{\pi P_o D^4}$$

$$C = B P_o$$

The λ_o or β_o for each volume is found by adding the λ_o or β_o for each tubing length between the source and the volume under consideration. Thus, from Figure 4,

$$\lambda_o\big]_{V_2} = \lambda_{o1} + \lambda_{o2}$$

$$\lambda_o\big]_{V_4} = \lambda_{o1} + \lambda_{o3} + \lambda_{o4}$$

$$\lambda_o\big]_{V_5} = \lambda_{o1} + \lambda_{o3} + \lambda_{o5}$$

Values of these lag constants for any altitude other than sea level may be determined from Figure 3. Equation (19) will yield the acoustic velocity after which the total lag error may be calculated from one of the relations below.

$$\left.\begin{aligned}\Delta P &= \left[\lambda + \frac{\ell}{a}\right]\dot{P} \\ \Delta H &= \left[\lambda + \frac{\ell}{a}\right]\dot{H}\end{aligned}\right\} \qquad (22)$$

3.4 Pitot-Static Tubes

The pitot-static tube, because of its location at the pressure system inlet, greatly influences the response of the entire system. Calculations made in the course of the WADC study indicated that the pitot tube can, in certain situations, contribute as much as 75% of the total lag of a static pressure system. As in numerous other cases, the design of a pitot-static tube is subject to considerable compromise. For instance, to achieve accurate static pressure measurement it is desirable to have pressure ports of small size. But from the standpoint of lag error, there should be one port having a diameter equal to the tubing ID so as to offer a minimum added resistance. Another significant point of compromise is the static pressure chamber within the pitot tube. To obtain a small over-all pitot tube size and the resulting desirable aerodynamic and de-icing characteristics, many designs employ annular static pressure chambers which surround the total pressure tube. It is readily apparent that this arrangement results in a high

frictional level since there are two surfaces over which the fluid must move.

To determine the degree of response degradation due to an annular chamber, both types of tubes (circular and annular) were compared. The analytical expression for the laminar flow pressure gradient in an annular cross-section is found by applying the proper boundary conditions to the Navier-Stokes equation. The result, as shown in Derivation Summary 3, is

$$\frac{dP}{dX} = -\frac{32\,\mu\,v}{D_1^2 + D_2^2 - \dfrac{D_1^2 - D_2^2}{\ln \dfrac{D_1}{D_2}}} \tag{23}$$

where D_1 and D_2 are, respectively, the outer and inner diameters of the annulus. Further development of equation (23) will yield an expression, analogous to equation (21), for an annular tube.

$$\Delta P_{f\ell} = \frac{128\,\mu\,\ell}{\pi\left[D_1^4 - D_2^4 - \dfrac{(D_1^2 - D_2^2)^2}{\ln \dfrac{D_1}{D_2}}\right]}\left[V_d + \frac{V_\ell}{2}\right]\frac{\dot{P}}{P} \tag{24}$$

Thus, from equations (21) and (24) it is seen that an annular tube has an equivalent circular diameter which is given by

$$D_{eq}^4 = D_1^4 - D_2^4 - \frac{(D_1^2 - D_2^2)^2}{\ln \dfrac{D_1}{D_2}} \tag{25}$$

A number of interesting comparisons can be made with the aid of equation (25). First, consider an annular tube with a cross-sectional area equivalent to that of 1/4 OD X .035 tubing. Assume also that D_2 = .25 inch. Then D_1 = .308 and D_{eq} is .0914 or approximately 3/32 inch. As a second example, assume a similar arrangement except that the cross-sectional area is equal to that of 3/8 OD X .035 tubing. In this case D_1 = .396 and D_{eq} = .19 (approx. 3/16). To obtain an equivalent diameter of .18 (1/4 X .035) with the same D_2 as before (1/4) would require a D_1 of about .38 inch. For the case where a 3/16 OD total pressure tube could be utilized. D_2 could be reduced to approximately .35 inches and still retain D_{eq}=.18. These figures indicate that, for tubes of equal resistance, the annular chamber offers no significant space advantage.

The sketches below illustrate this conclusion.

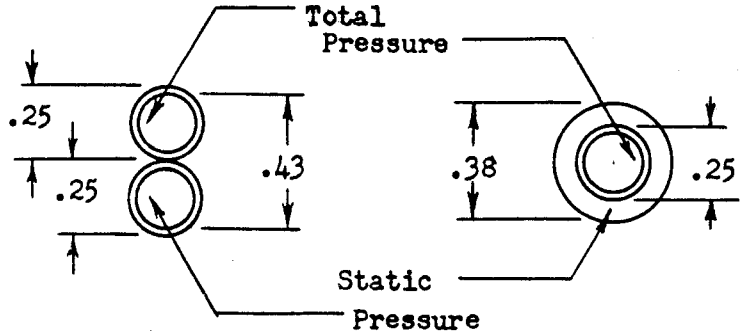

The system designer is often willing to accept a slight response degradation inside the pitot tube since it is comparatively short in length. The annular arrangement then becomes very advantageous. It should be remembered, however, that the criterion for selection of an annular tube size is the equivalent circular diameter and not the actual cross-sectional area.

3.5 Specific System Arrangements

It can be seen from equation (21) (Article 3.3) that the three major geometry parameters affecting lag error are tubing ID, tubing length, and internal volume. Thus, improvement in the response of a given system can be achieved by decreases in volume, or line length, or by increases in ID. One phase of the WADC investigation was devoted to analytical comparisons of the lag of various system arrangements when applied to an actual installation. Figure 5 illustrates seven different arrangements which could be utilized for the static pressure system of a high performance aircraft. These systems offer varying amounts of response improvement over the so-called "standard" arrangement wherein 1/4 OD tubing is used throughout.

The layouts of Group A require the use of two pitot-static tubes or one tube having two separate static pressure sources. This reduces the volume downstream from each source. Group A layouts are preferred in some cases, particularly flight test installations, because each instrument volume is supplied by a separate source. Additional equipment can be added without affecting the lag of the complete system. For production aircraft, however, this type of layout has a distinct disadvantage. This is brought about by the fact that, for supersonic vehicles, a nose boom provides the only acceptable location for a pitot-static tube. Two separate tubes would be awkward to mount on a single boom. Moreover, a dual source tube is, in general, considerably larger and more complicated than a normal tube. This results in degraded aerodynamic performance and necessitates an increased amount of heat for de-icing purposes.

Group B systems offer possibly the simplest means of improvement since only a change in tubing size is involved. The common line, having a large downstream volume, is the obvious starting point for any improvement of this nature. Group C represents another method of decreasing the lag contribution of the common line by locating the main junction directly aft of the nose boom.

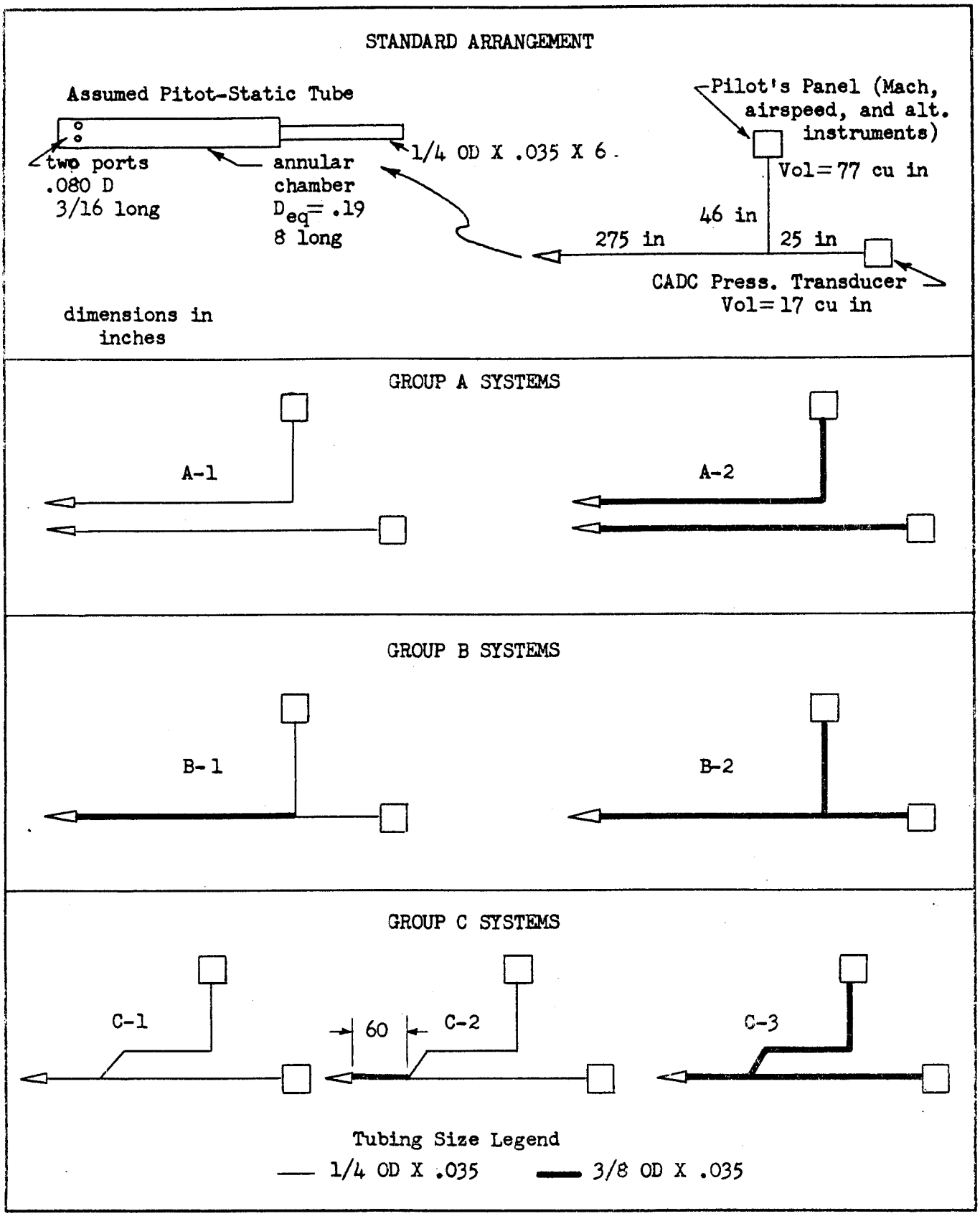

Figure 5 Various System Arrangements Compared (Theoretically) With Standard Layout

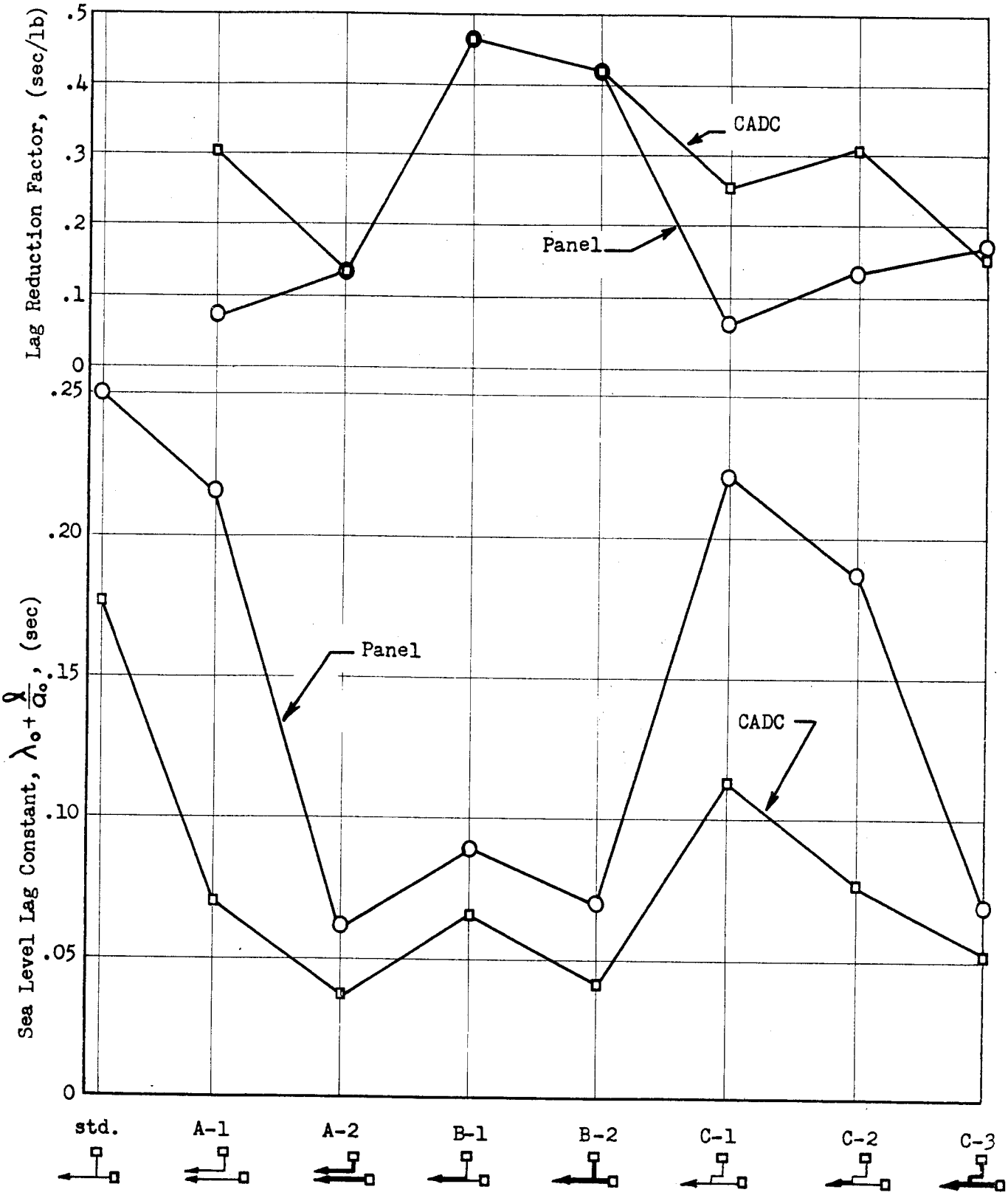

Figure 6 Comparison of Calculated Lag Characteristics of Eight Static Pressure System Arrangements

Figure 6 compares the sea level lag constant ($\lambda_o + \frac{\ell}{a_o}$) for each system in Figure 5. Four of the seven systems (A-2, B-1, B-2, and C-3) show significant lag improvement. Of the remaining three layouts, two (A-1 and C-2) have reduced the CADC lag considerably but have had little effect on the panel lag.

Frequently a particular arrangement cannot be chosen on the basis of lag reduction alone because, as Figure 6 implies, some layouts, though very attractive response-wise, may introduce weight problems and/or installation difficulties. In order to more thoroughly evaluate a group of arrangements, it was found advantageous to make use of another parameter which was termed the "lag reduction Factor". This factor, plotted also in Figure 6, is defined for a given arrangement as "the amount of lag decrease (in sec.) from the standard layout per pound of system weight increase over the standard".

It is interesting to note that arrangement B-1, while not the most desirable from lag considerations alone, does yield the greatest amount of response improvement per unit of weight increase. Companion arrangement B-2 also ranks high on this scale. The converse is true for layout A-2 which has the best response. This system rates fairly low, indicating that the lag improvements carry greater weight penalties than B-1 or B-2. These same remarks apply to system C-3. Sample lag calculations for Fig. 6 are presented in Appendix II.

This article concludes the Analysis section of the report. The preceding discussions have been presented to demonstrate the utility of calculations and comparisons in pressure system design.

SECTION IV

EXPERIMENTAL PHASE

4.1 Test Equipment and Techniques

The objectives of the experimental phase of the WADC lag study were twofold. First, it was desired to determine the degree of validity of the fundamental flow assumptions stated in Article 3.2. The second objective, an extension of the first, was to compare the actual lag characteristics of various arrangements with those predicted by the analytical method previously demonstrated.

The general lag test procedure consisted of applying a ramp input function to a test chamber (in which the inlet of a simulated pressure measuring system was located) and recording the pressure drop between the chamber and various instrument volumes by means of 1 psi differential pressure transducers. A 15 psi differential transducer was used to monitor the chamber pressure with respect to ambient. The outputs of the transducers were recorded by oscillograph. Figures 7 and 8 show the general arrangement of the test equipment.

Some difficulty was encountered in the production of a satisfactory ramp input. The first method attempted was similar to the procedures reported by Smith (ref. 13) and Newman (ref. 8). In this scheme a manually controlled valve admitted air to the test chamber. The input rate was established by means of a mercury manometer and a pointer moving at constant speed up the manometer scale. The valve operator attempted to equalize the rates of the pointer and mercury column. Test runs made in this manner yielded data with considerable scatter. In particular, the 1 psid transducer outputs exhibited severe oscillations which were attributed to rate variations resulting from the manual control. The sensitivity of these transducers was such that the nonlinearities were greatly magnified. It was obvious that some automatic method of ramp function production was necessary.

In this respect a technique developed by Reid and Campbell (ref. 10) appeared very promising. This procedure made use of a choked orifice which passed air into the test chamber at a constant rate. In the WADC tests a 20 psig driving pressure was also used to achieve the critical orifice pressure ratio at test chamber pressures near ambient. In addition a stablization chamber was incorporated into the system to remove supply pressure fluxuations. During the test runs the simulated system and the main chamber were evacuated to a pressure altitude of 80,000 feet and isolated for leakage checks. (Leakage was held to a maximum of 0.002 psi over a 10 minute period.) The intake valve was then opened, allowing air to enter the test chamber through the metering orifice. Concurrently with the opening of the valve the oscillograph was energized and the response recorded. Four interchangeable orifices were used to achieve ramp input rates of 0.1, 0.2, 0.3, and 0.4 psi/sec. The accuracy of the transducer, amplifier, oscillograph combination was found to be .004 psi.

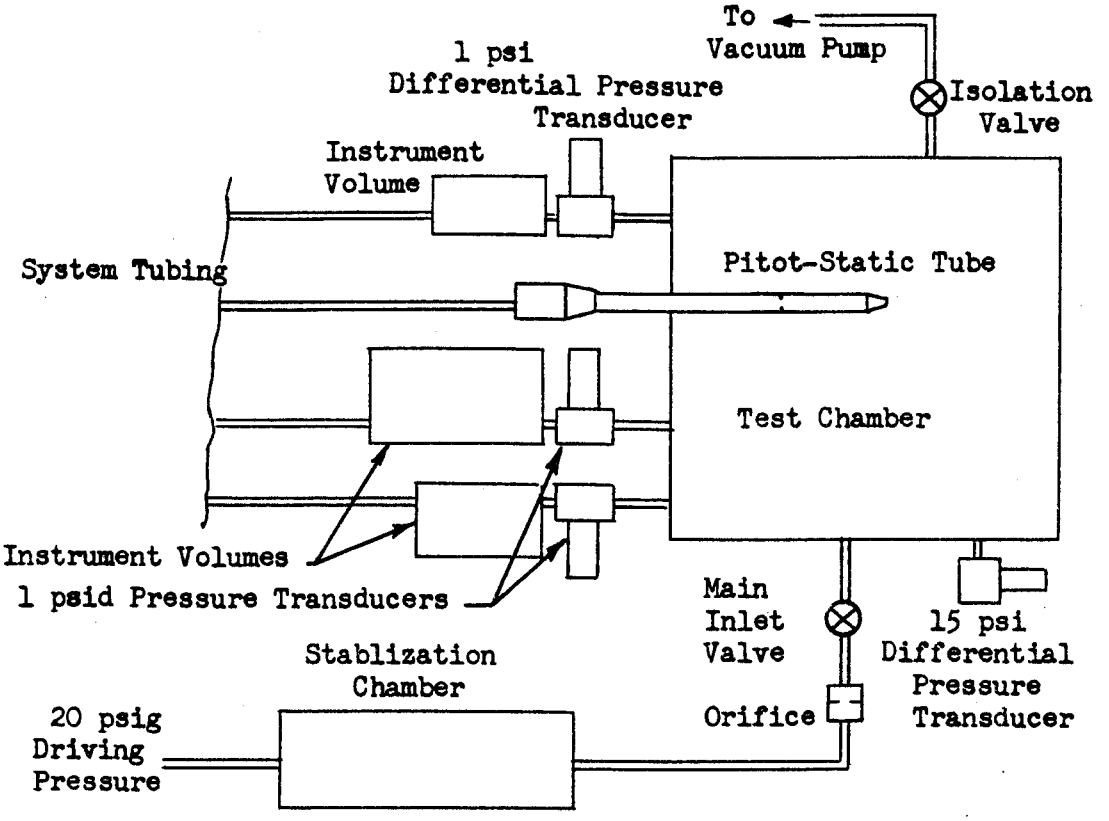

Figure 7 General Arrangement of Test Apparatus

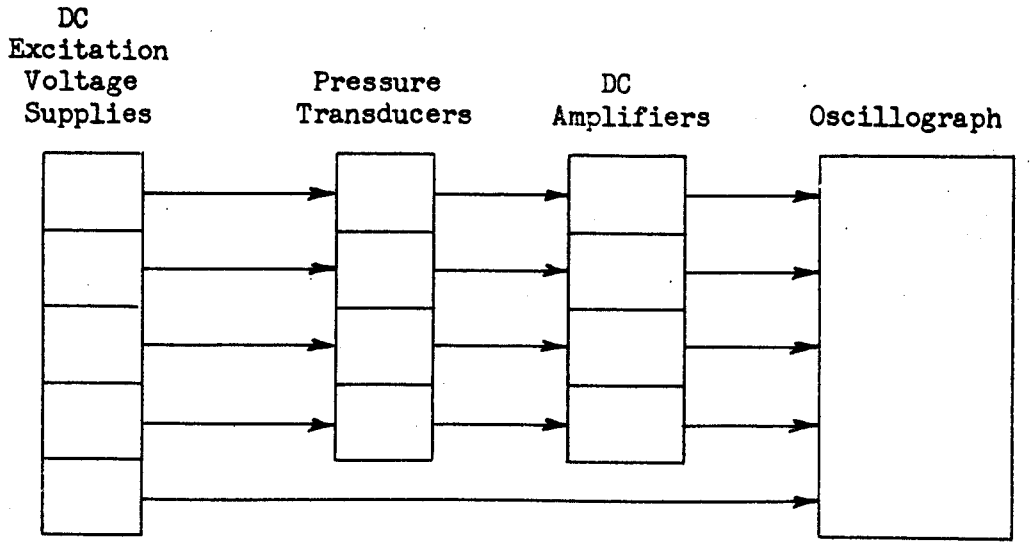

Figure 8 Electrical Diagram

4.2 Arrangements Considered

For the experimental phase, the static pressure system of a single-engine, high-performance aircraft was chosen for study. Manufacturer's drawings were obtained to show line lengths, type and location of fittings, and instrument volumes. This information was utilized in fabricating the test systems. Figure 9 illustrates the arrangements which were investigated. Systems 1, 2, and 3 represent different approaches to the same installation while system 4 incorporates a second panel volume. Systems 5 and 6 have only one panel and the CADC volume. These latter arrangements were also utilized to determine the lag contributions of the various types of pitot-static tubes shown in Figure 10.

4.3 Test Results and Analysis

The following parameters were recorded (or calculated from raw data) for each test run: ramp input rate, test chamber pressure, pressure lags for each instrument volume, ambient temperature, and ambient pressure. A sample data sheet is shown in Table 1.

Before the data analysis began, calculated acoustic lag values were subtracted from each recorded pressure drop so as to leave only the viscous lag. These frictional lag values were then plotted as a function of inlet (chamber) pressure. A typical plot, utilizing the data of Table 1, is shown in Figure 11. The significant influence of inlet pressure magnitude upon lag is again quite obvious, as is the effect of inlet pressure rate.

Viscous lag values taken from these curves of ΔP_f vs. P were subsequently graphed in the manner described in Article 3.2,i.e., ΔP_f vs. $\dot{P}/P$. Figures 12 through 36 present the experimental results in this form. Shown also on each plot is a straight line representing the calculated frictional lag for the instrument volume under consideration. The slope of this line is, of course, equal to the value of β .

It will be noted that the ΔP_f vs. P curves could have been omitted and the data plotted directly in ΔP_f vs. $\dot{P}/P$ form. It was found, however, that the two-curve method generally gave a more accurate indication of a system's lag characteristics by eliminating the influence of lag values which were clearly erroneous.

A number of interesting facts emerge from an examination of Figures 12 through 36. First, it is seen that theory and experiment are in reasonable agreement at low values of $\dot{P}/P$. Where there are discrepances, the calculated values are conservative. These variances are probably the result of differences between the actual geometry and the dimensions upon which the calculations are based. (In particular, the diameters of pitot tube chambers were found to be critical.) It is also noted that as $\dot{P}/P$ increases, the experimental lines on many of the curves bend upward and away from the calculated slopes. This nonlinearity, previously observed by Smith, is believed to be the result of a change from laminar conditions to transitional or semi-turbulent flow within the system. It also illustrates the underlying cause for this type of plot, viz., $\dot{P}/P$ is a function of the flow Reynold s number, This relationship is seen more clearly from a

(text continued on page 39)

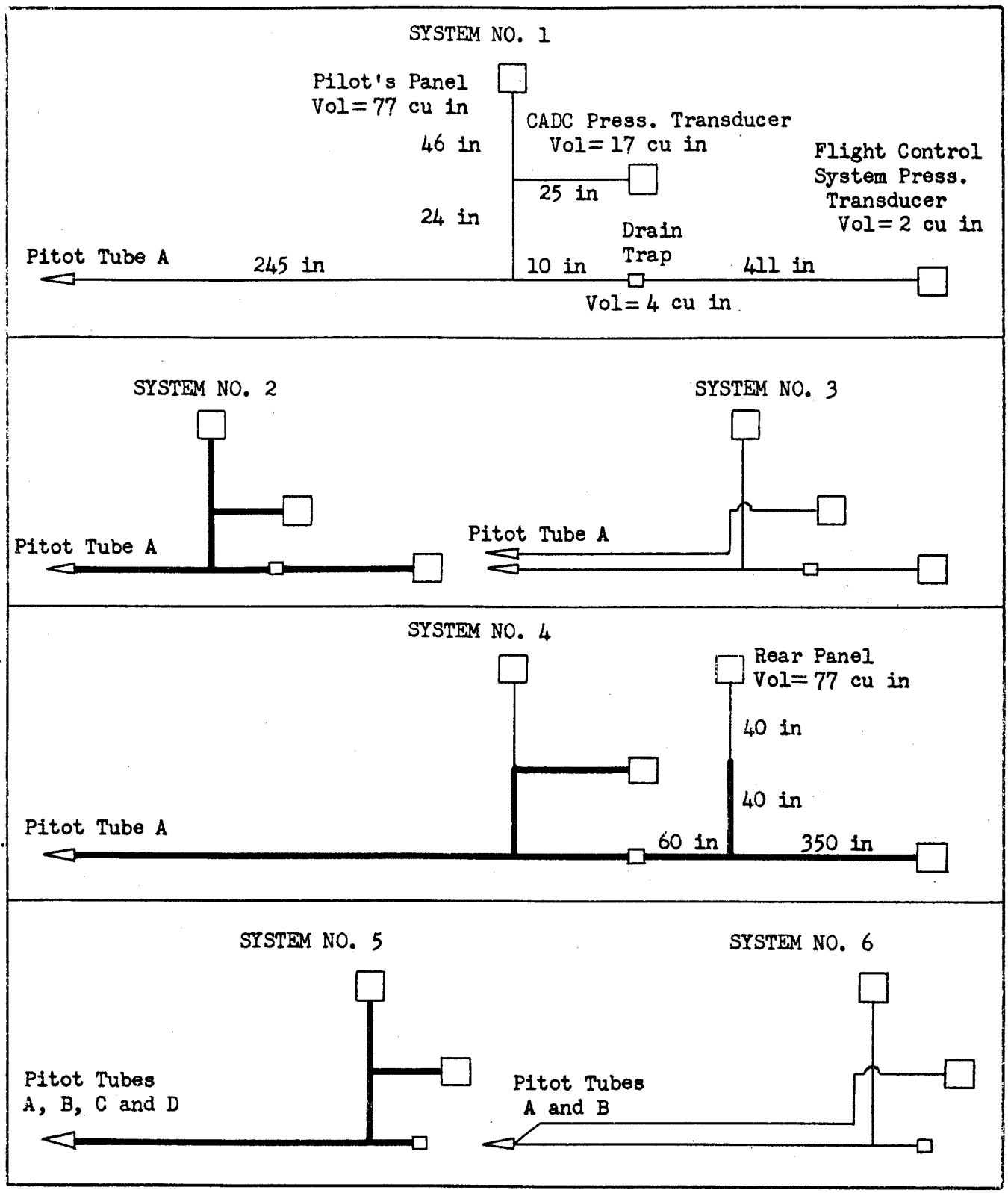

Figure 9 Arrangements Tested During Experimental Phase (See Fig. 10 for pitot tube dimensions)

PITOT-STATIC TUBE A

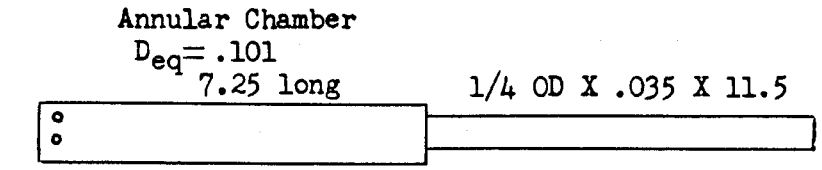

two ports
.070 D
.157 long

PITOT-STATIC TUBE B

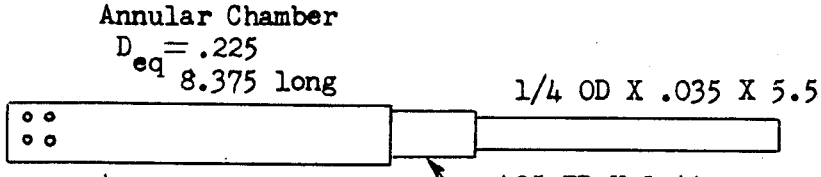

four ports
.080 D
3/16 long

PITOT-STATIC TUBE C

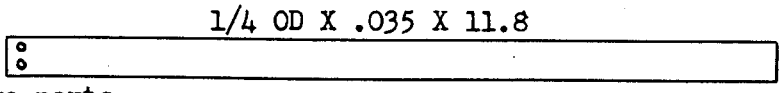

two ports
same size as tube B

PITOT-STATIC TUBE D
(AN 5816)

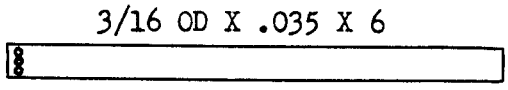

ten ports
.040 D
3/16 long

Figure 10 Various Pitot-Static Tube Designs Considered During Experimental Phase (All dimensions in inches)

TABLE 1

Sample Test Data Sheet for System No. 1

Ambient pressure 29.3 in. Hg. abs.
Ambient Temperature 25°C

Test Chamber Pressure (psia)	Ramp Input Rate (psi/sec)	Total Lag Error (psid)		
		Pilot's Panel	CADC Transducer	Control System Transducer
4.18	0.441	1.050	0.998	0.984
5.31		0.730	.698	.700
6.43		.540	.500	.508
9.64		.350	.326	.350
11.79		.270	.246	.270
13.05		.210	.210	.220
3.32	0.313	0.878	0.838	0.842
4.11		.668	.640	.660
6.27		.342	.326	.342
8.69		.207	.220	.233
11.25		.150	.150	.159
13.39		.104	.112	.120
2.71	0.163	0.532	0.500	0.510
3.08		.425	.392	.418
4.28		.220	.218	.231
7.58		.096	.090	.118
10.19		.070	.070	.072
13.32		.050	.057	.056
2.18	0.101	0.360	0.345	0.352
2.58		.250	.242	.268
3.62		.132	.122	.128
6.51		.073	.065	.068
10.25		.050	.040	.046
13.39		.040	.033	.032

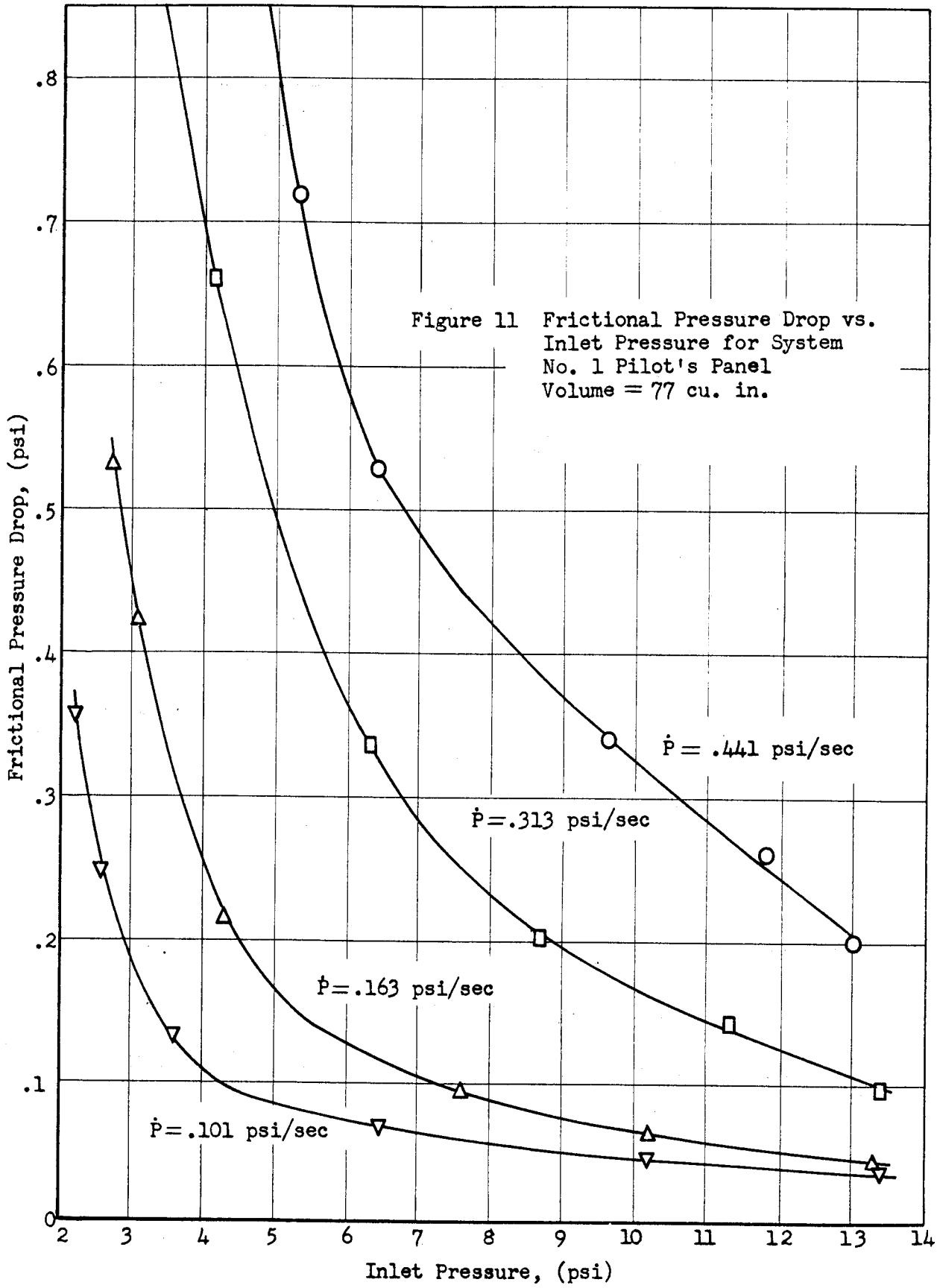

Figure 11 Frictional Pressure Drop vs. Inlet Pressure for System No. 1 Pilot's Panel Volume = 77 cu. in.

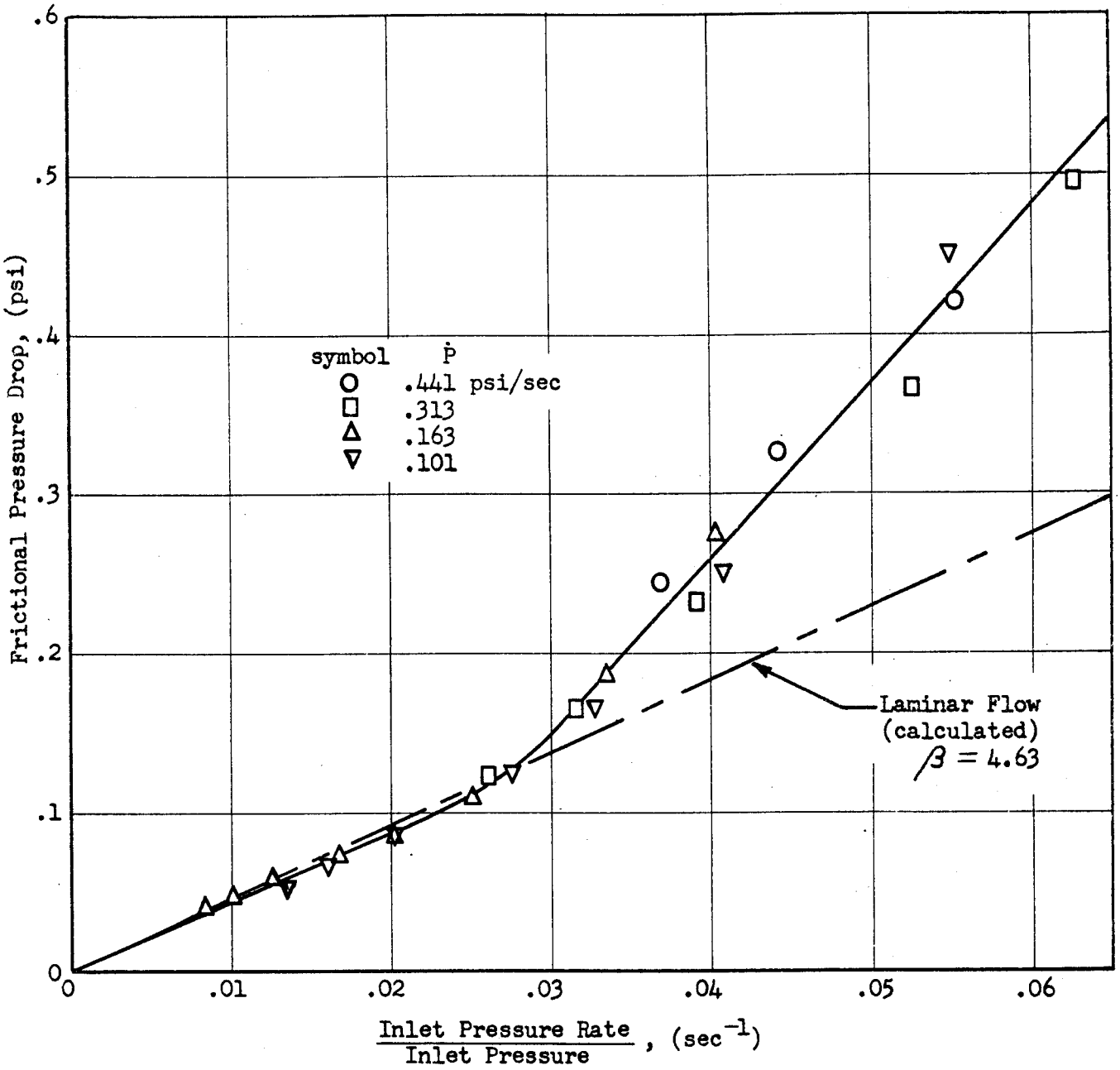

Figure 12 Frictional Pressure Drop vs. $\frac{\text{Inlet Pressure Rate}}{\text{Inlet Pressure}}$ for System No. 1 Pilot's Panel
Volume = 77 cu. in.

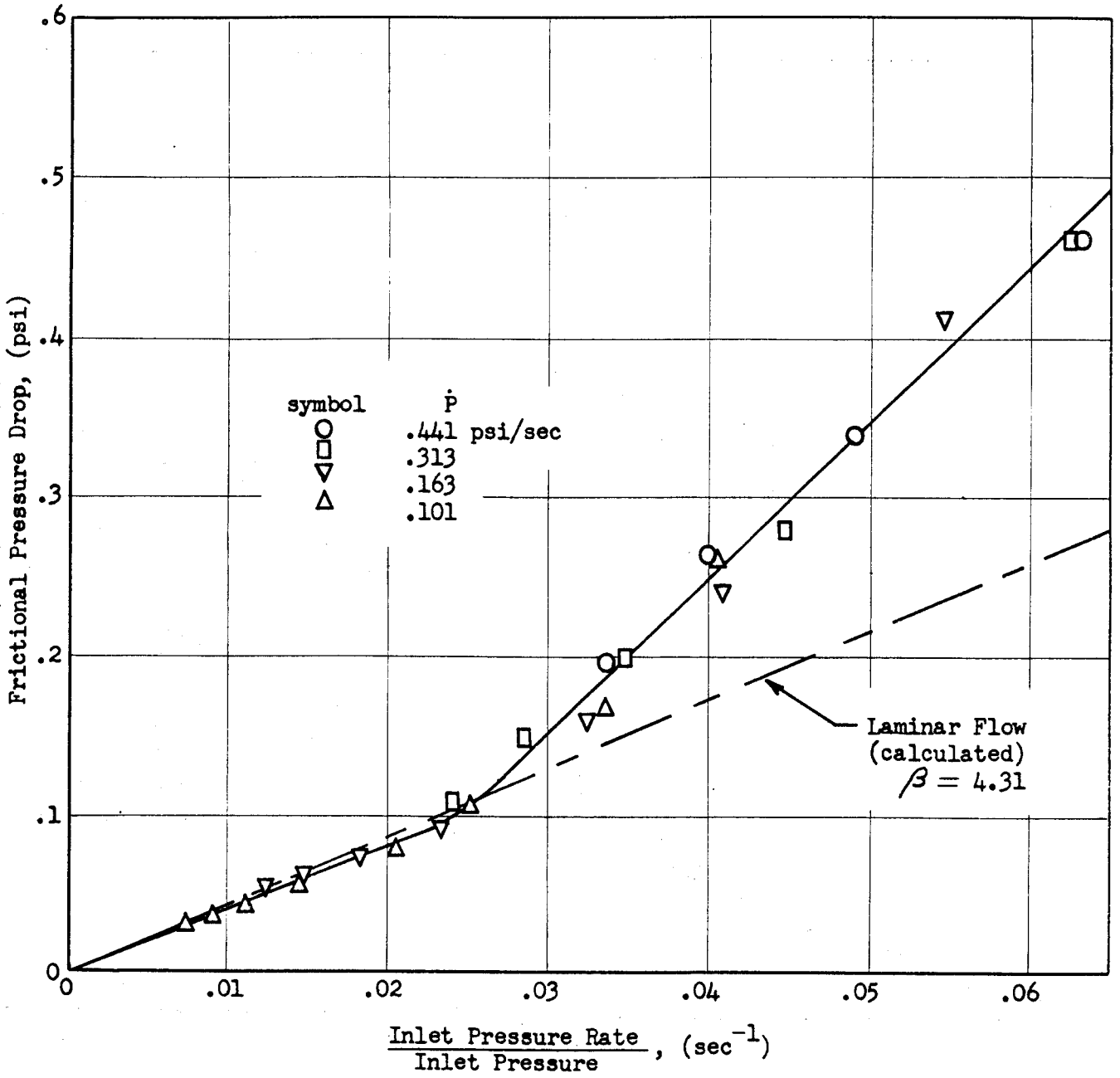

Figure 13 Frictional Pressure Drop vs. $\frac{\text{Inlet Pressure Rate}}{\text{Inlet Pressure}}$ for System No. 1 CADC Pressure Transducer Volume = 17 cu. in.

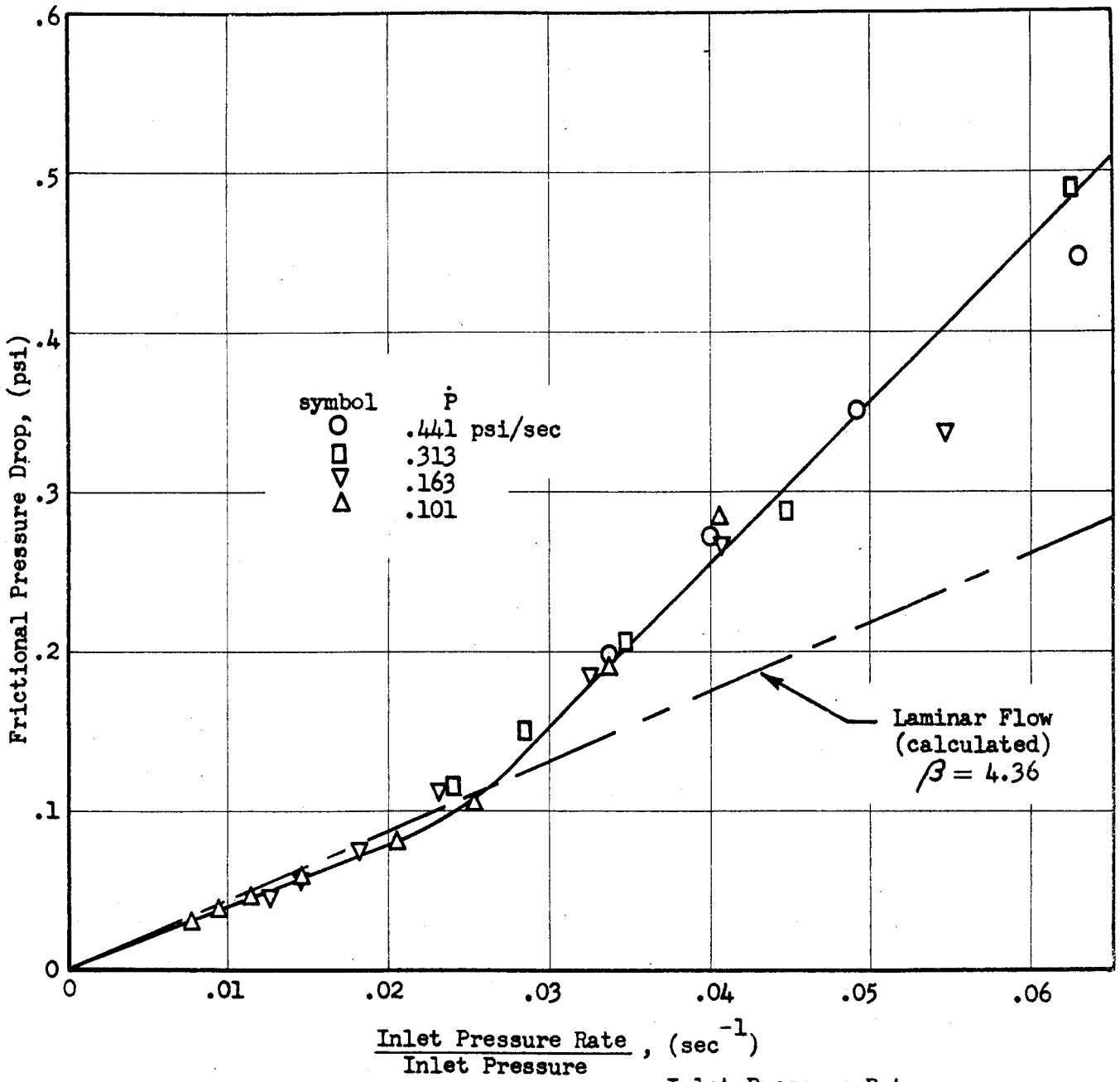

Figure 14 Frictional Pressure Drop vs. $\frac{\text{Inlet Pressure Rate}}{\text{Inlet Pressure}}$ for System No. 1 Control System Pressure Transducer Volume = 2 cu. in.

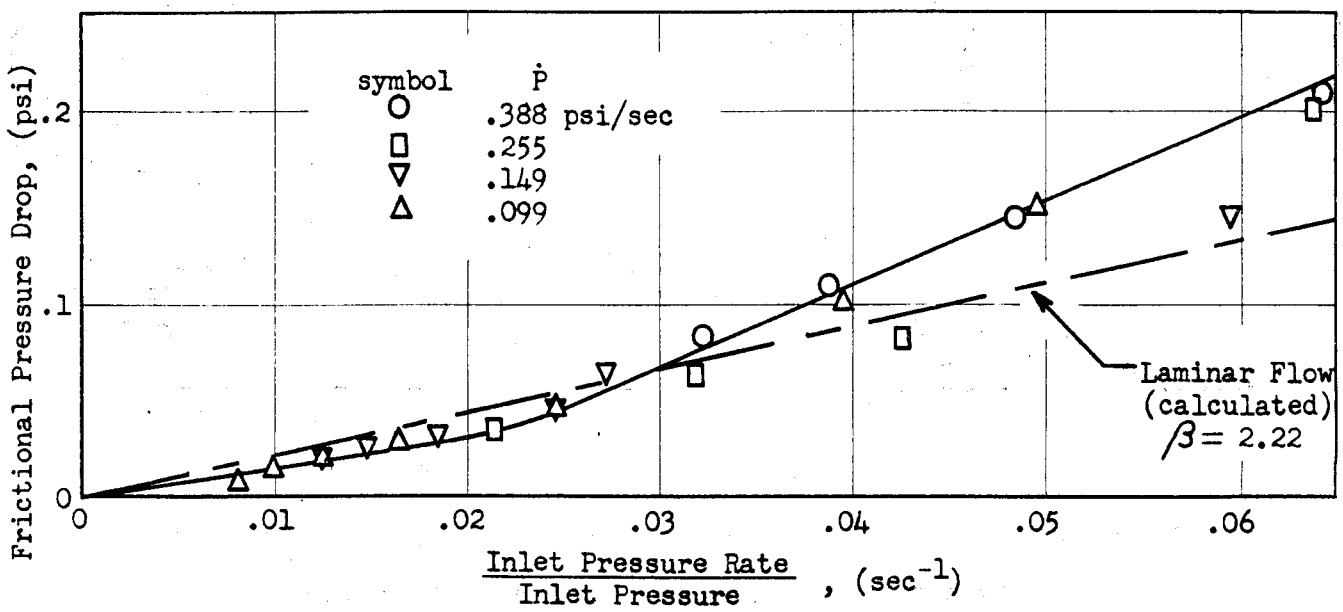

Figure 15 Frictional Pressure Drop vs. $\frac{\text{Inlet Pressure Rate}}{\text{Inlet Pressure}}$ for System No. 2 Pilot's Panel
Volume = 77 cu. in.

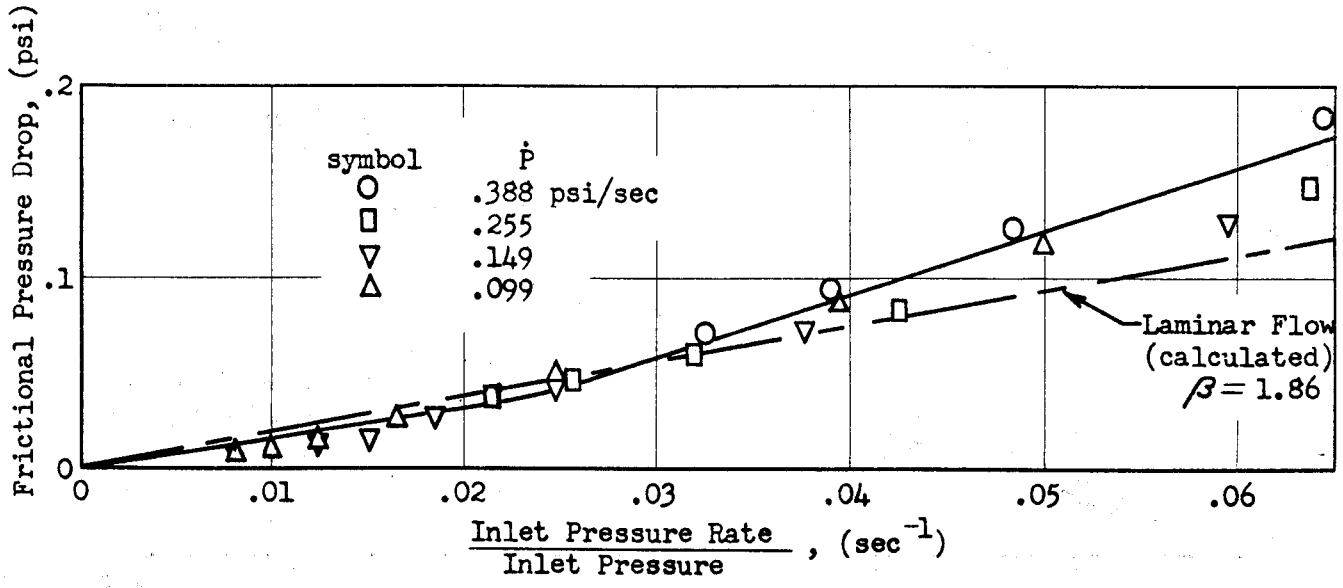

Figure 16 Frictional Pressure Drop vs. $\frac{\text{Inlet Pressure Rate}}{\text{Inlet Pressure}}$ for System No. 2 CADC Pressure Transducer
Volume = 17 cu. in.

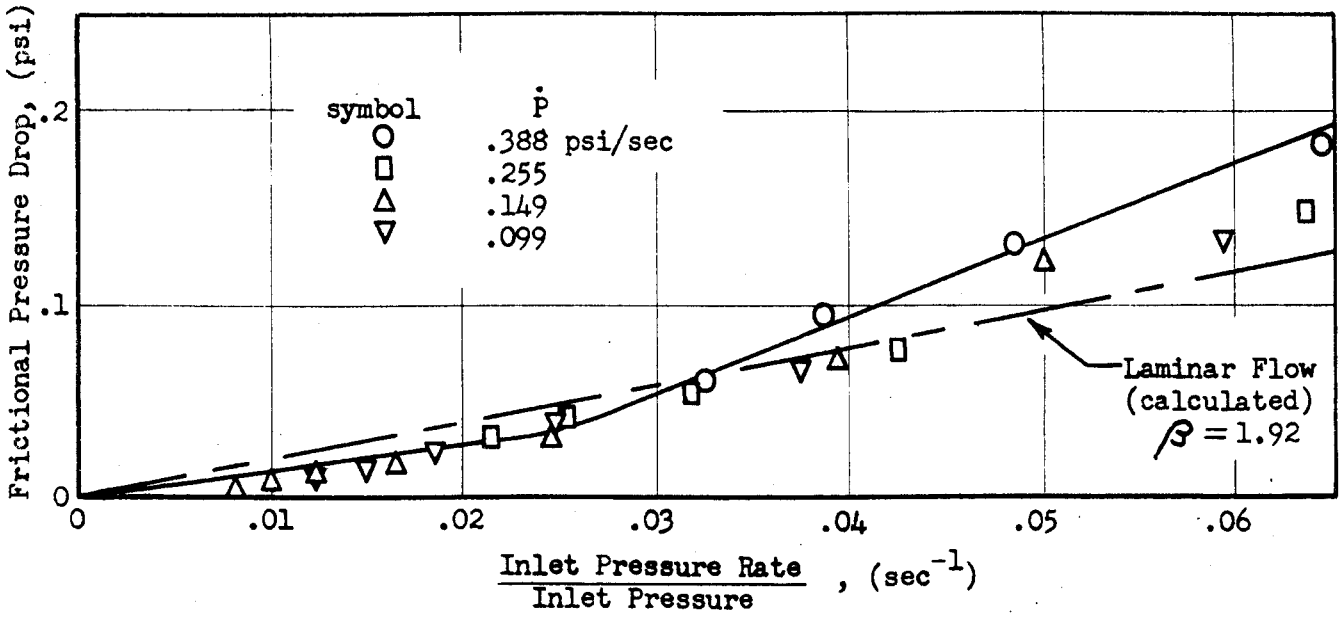

Figure 17 Frictional Pressure Drop vs. $\frac{\text{Inlet Pressure Rate}}{\text{Inlet Pressure}}$ for System No. 2 Control System Pressure Transducer Volume = 2 cu. in.

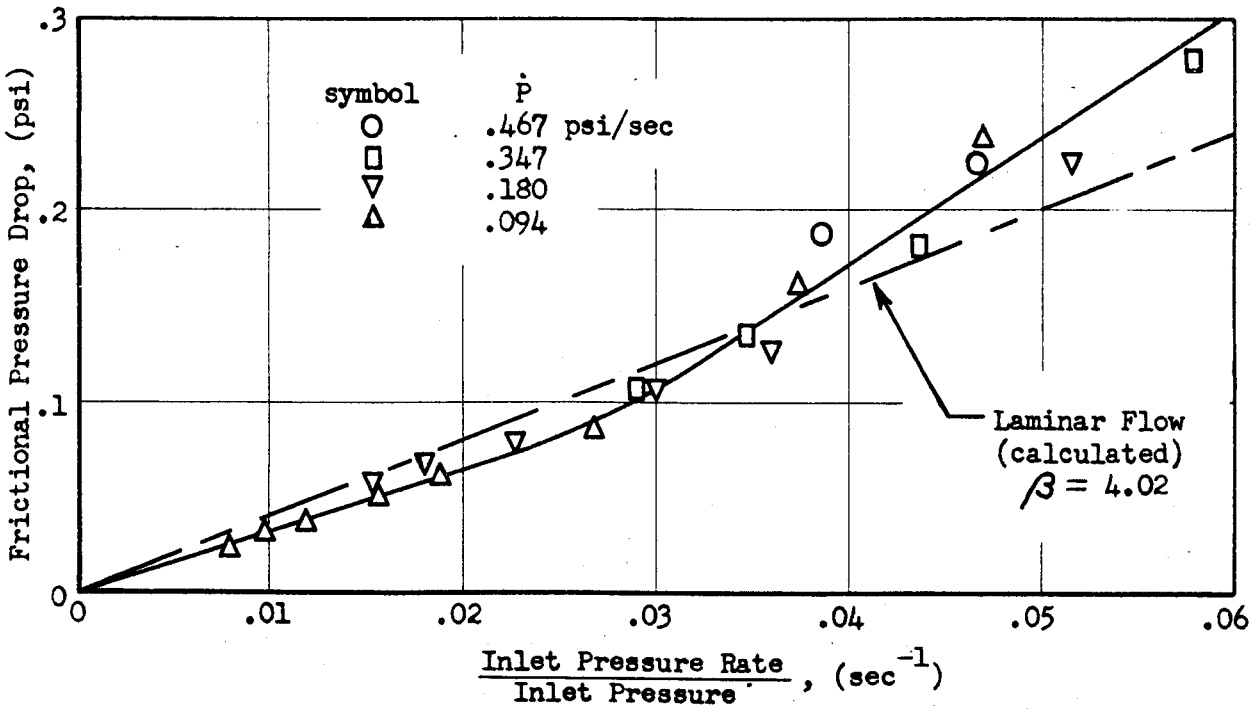

Figure 18 Frictional Pressure Drop vs. $\frac{\text{Inlet Pressure Rate}}{\text{Inlet Pressure}}$ for System No. 3 Pilot's Panel Volume = 77 cu. in.

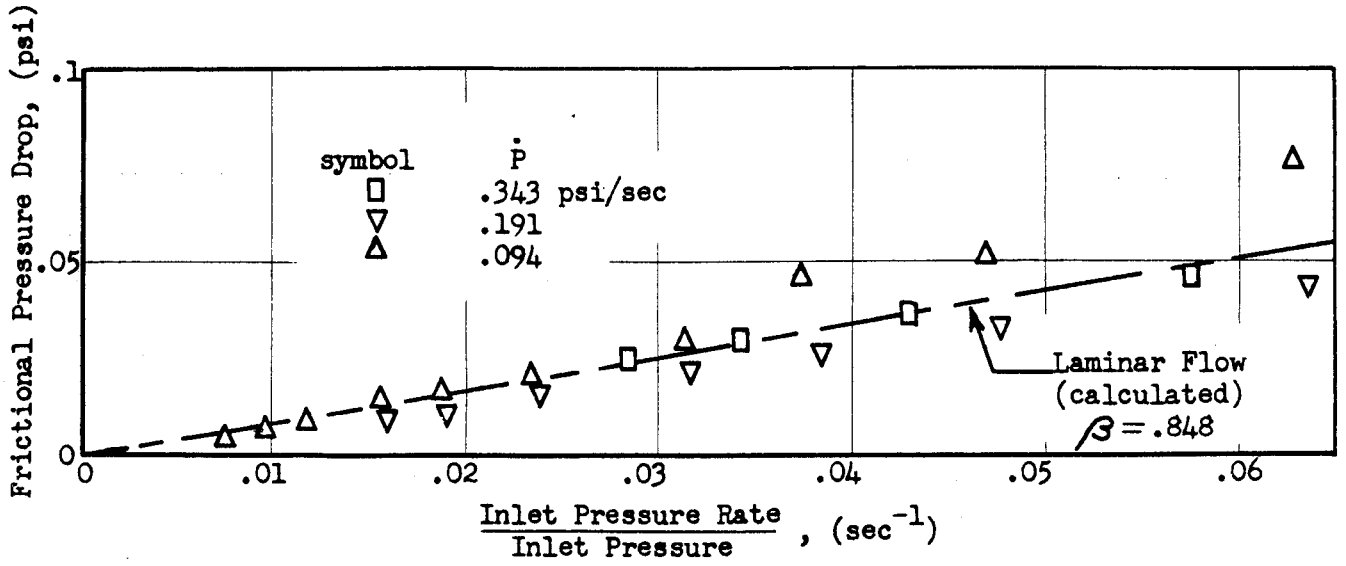

Figure 19 Frictional Pressure Drop vs. $\frac{\text{Inlet Pressure Rate}}{\text{Inlet Pressure}}$ for System No. 3 CADC Pressure Transducer Volume = 17 cu. in.

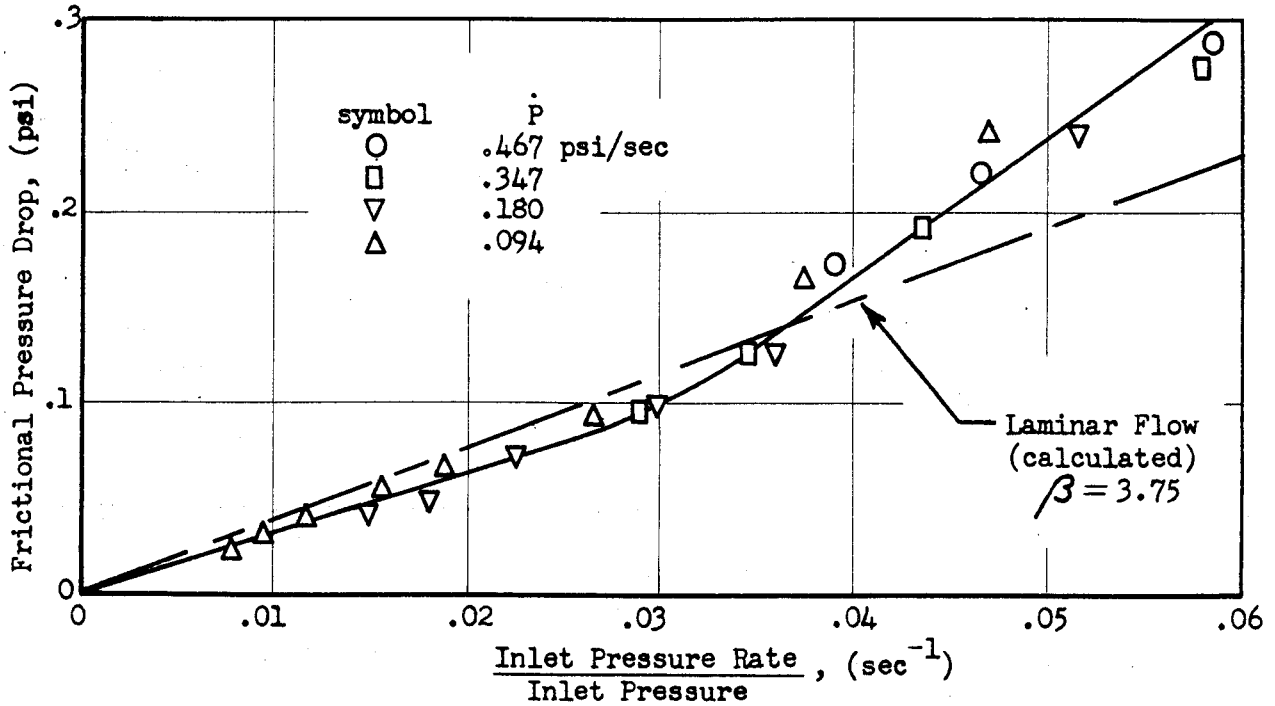

Figure 20 Frictional Pressure Drop vs. $\frac{\text{Inlet Pressure Rate}}{\text{Inlet Pressure}}$ for System No. 3 Control System Pressure Transducer Volume = 2 cu. in.

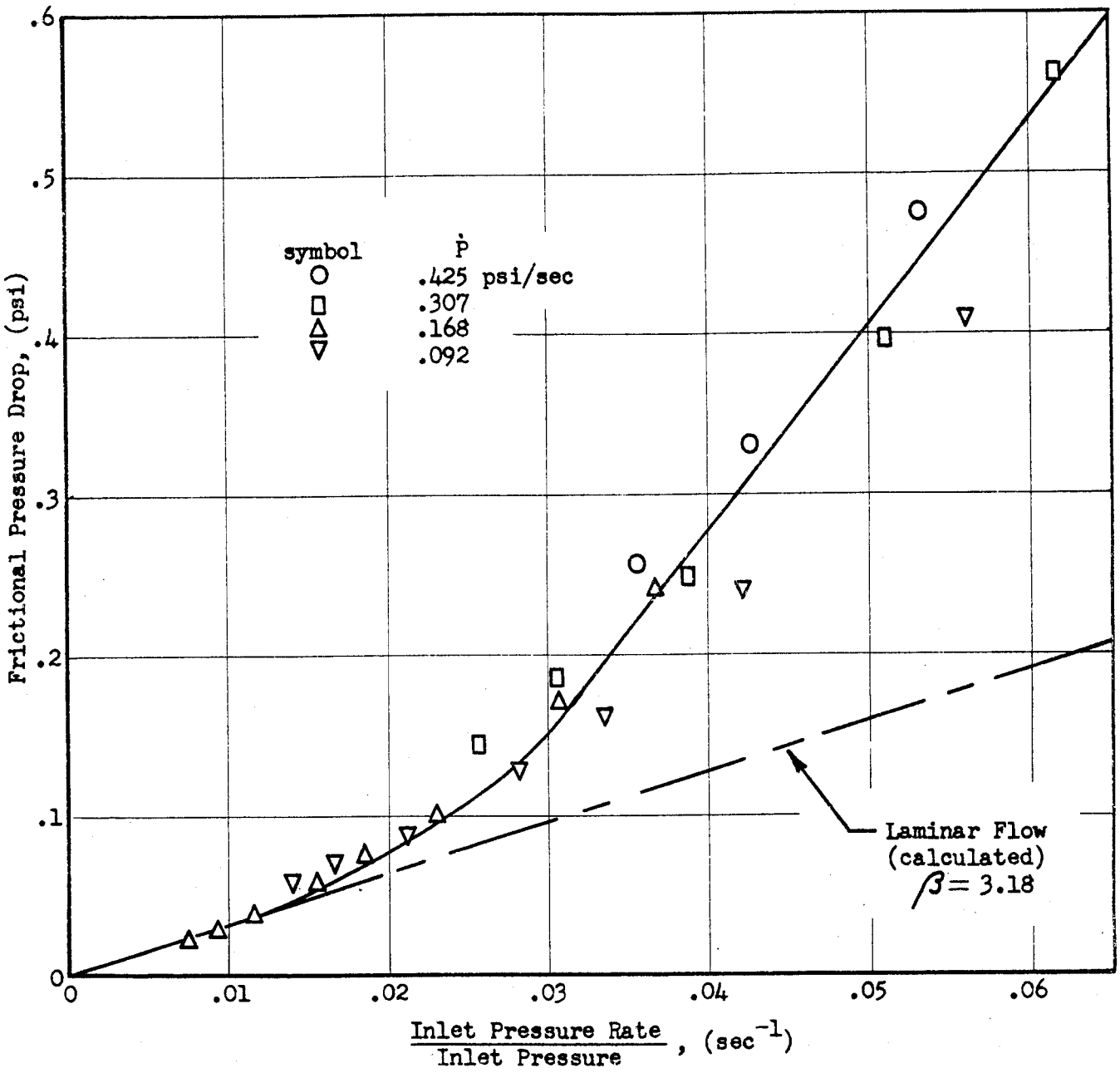

Figure 21 Frictional Pressure Drop vs. $\frac{\text{Inlet Pressure Rate}}{\text{Inlet Pressure}}$ for System No. 4 Front Panel
Volume = 77 cu. in.

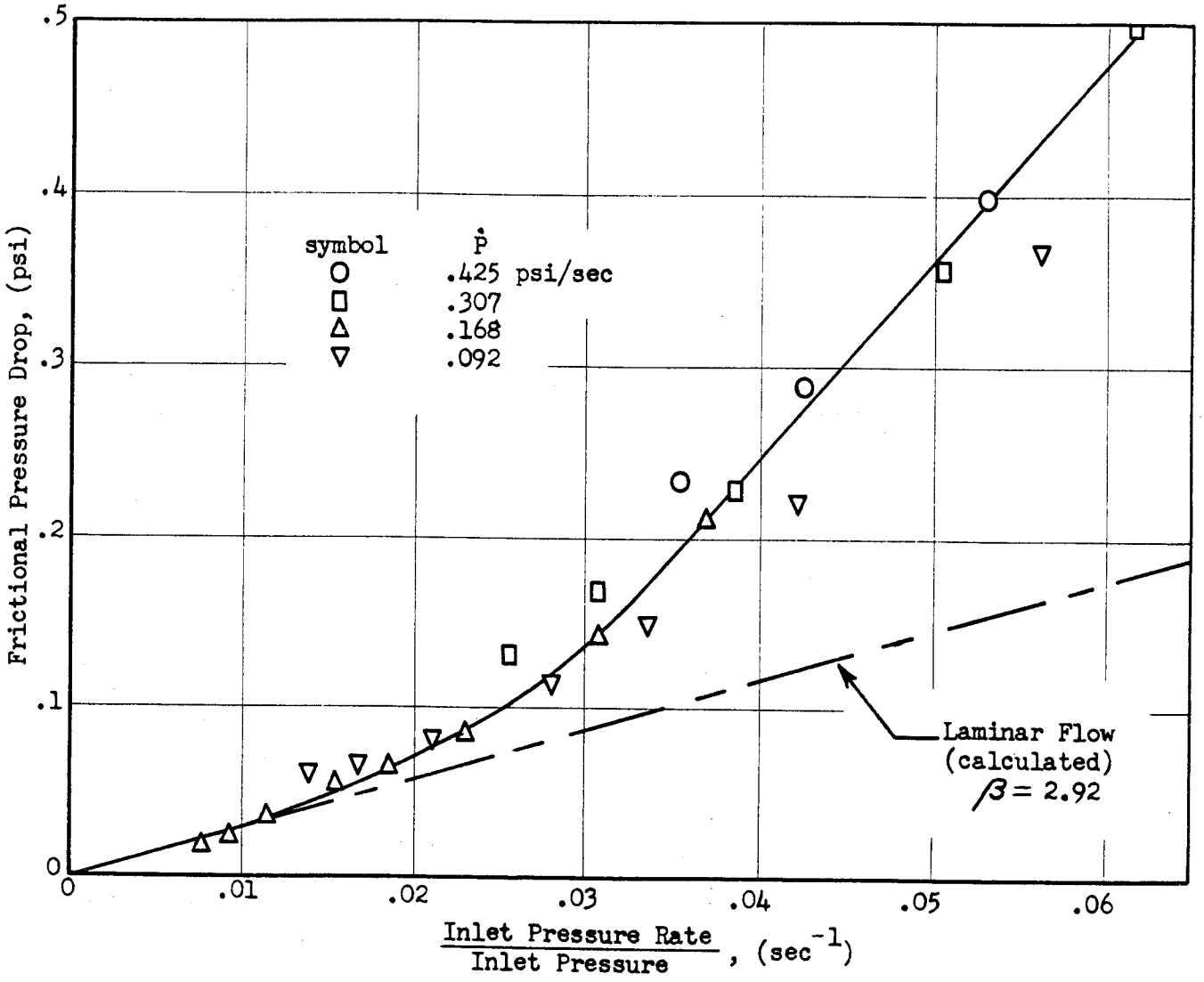

Figure 22 Frictional Pressure Drop vs. $\frac{\text{Inlet Pressure Rate}}{\text{Inlet Pressure}}$ for System No. 4 CADC Pressure Transducer Volume = 17 cu. in.

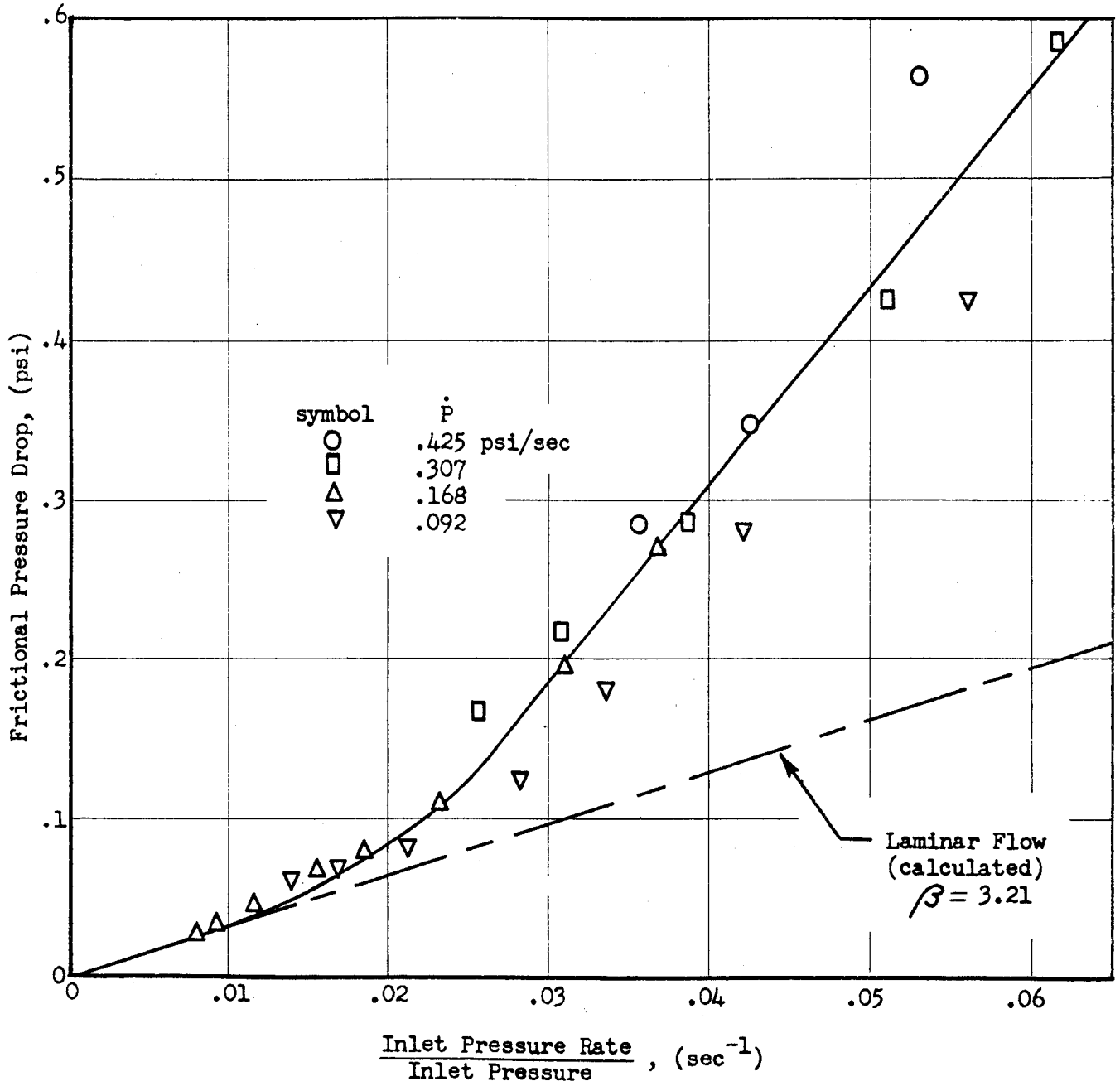

Figure 23 Frictional Pressure Drop vs. $\frac{\text{Inlet Pressure Rate}}{\text{Inlet Pressure}}$ for System No. 4 Rear Panel
Volume = 77 cu. in.

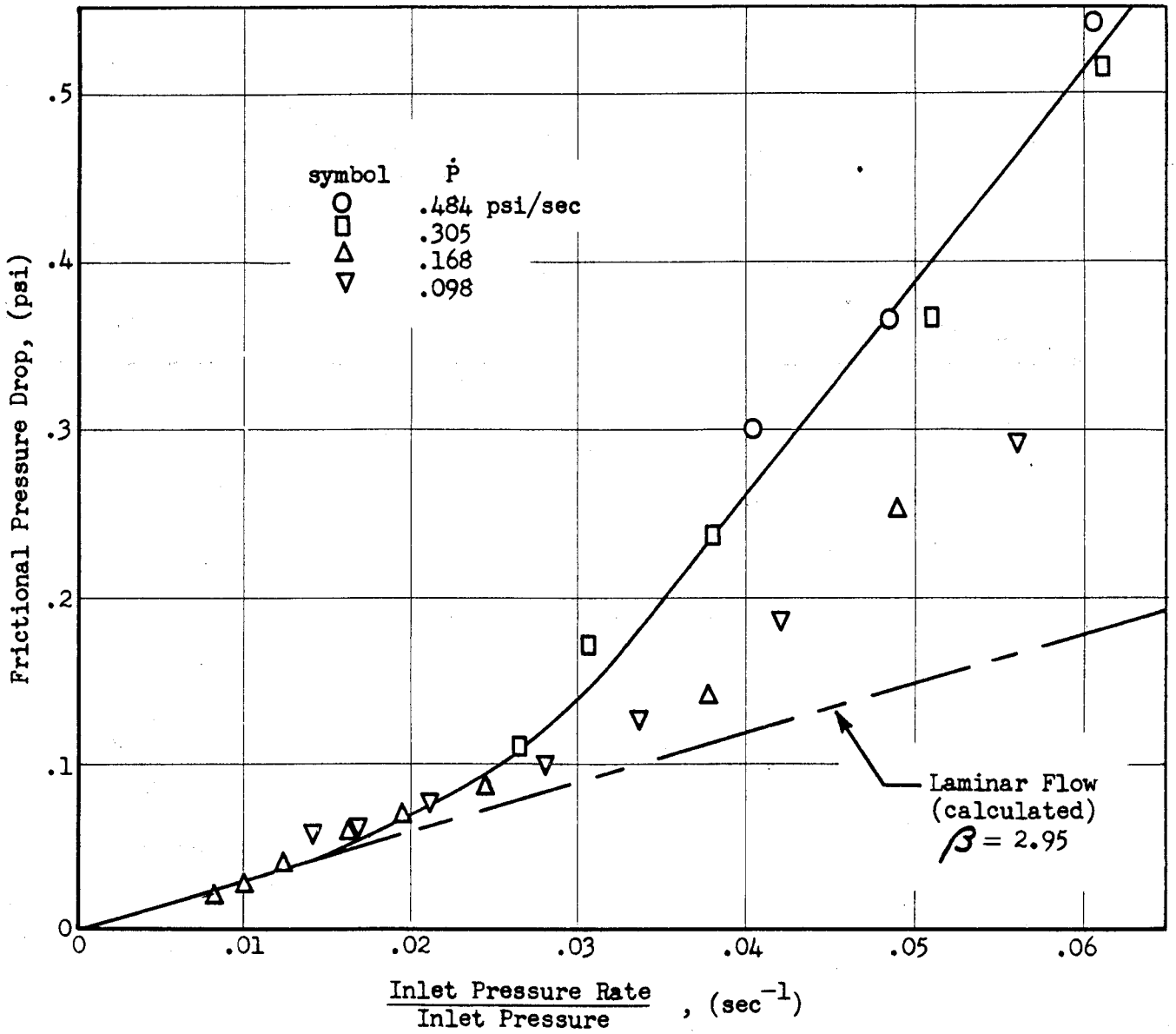

Figure 24 Frictional Pressure Drop vs. $\frac{\text{Inlet Pressure Rate}}{\text{Inlet Pressure}}$ for System No. 4 Control System Pressure Transducer Volume = 2 cu. in.

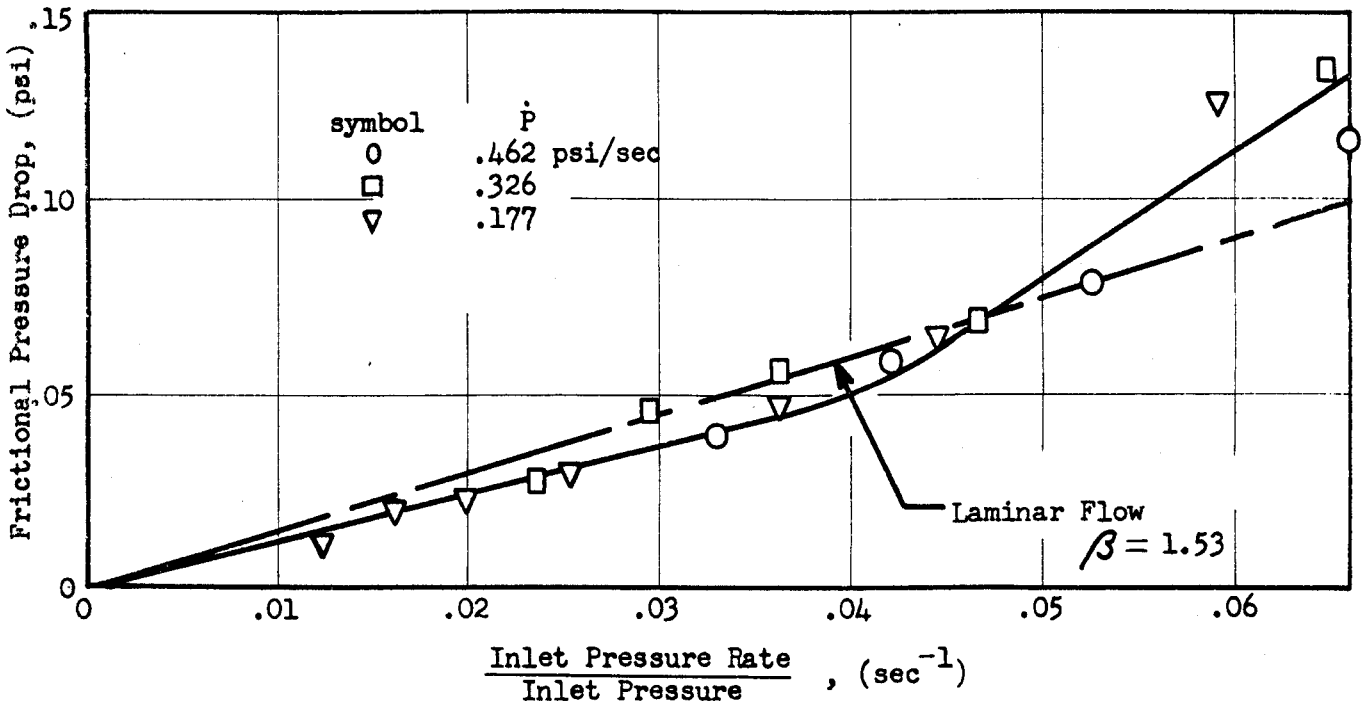

Figure 25 Frictional Pressure Drop vs. $\frac{\text{Inlet Pressure Rate}}{\text{Inlet Pressure}}$ for

System No. 5 Pilot's Panel
Volume = 77 cu. in. Pitot Tube A

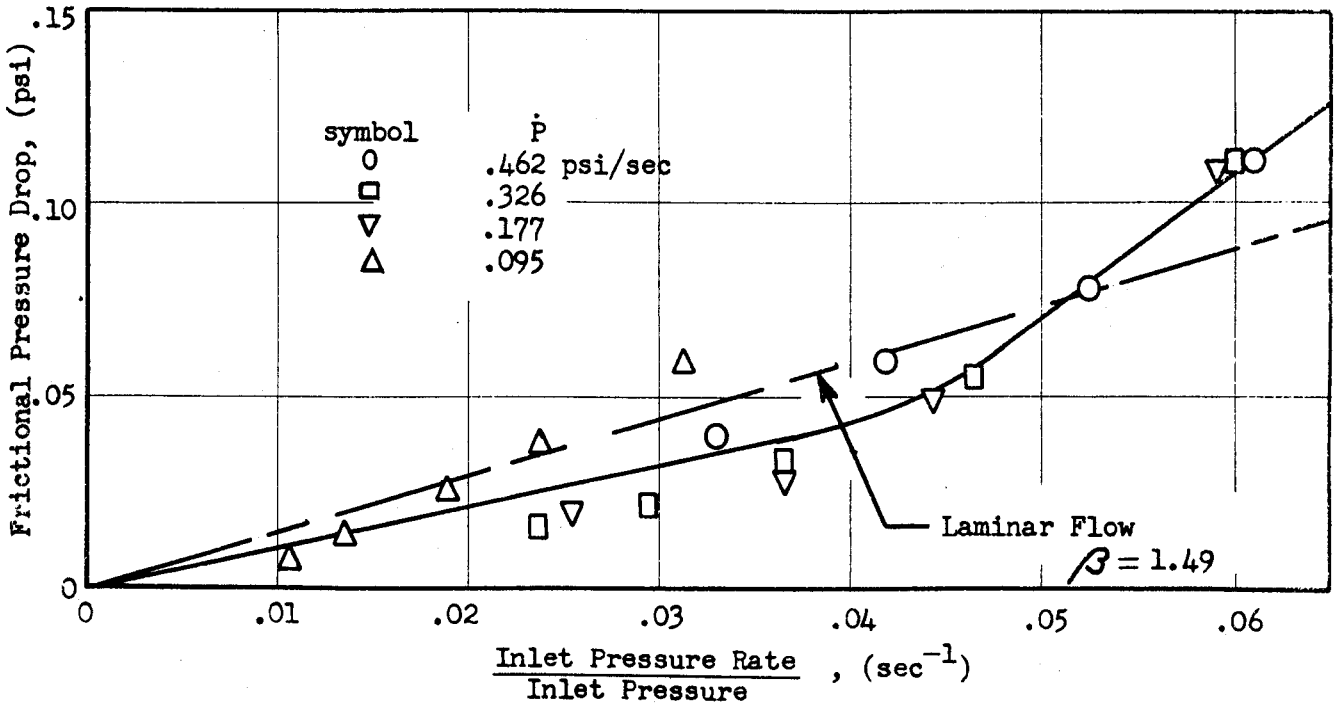

Figure 26 Frictional Pressure Drop vs. $\frac{\text{Inlet Pressure Rate}}{\text{Inlet Pressure}}$ for

System No. 5 CADC Pressure Transducer
Volume = 17 cu. in. Pitot Tube A

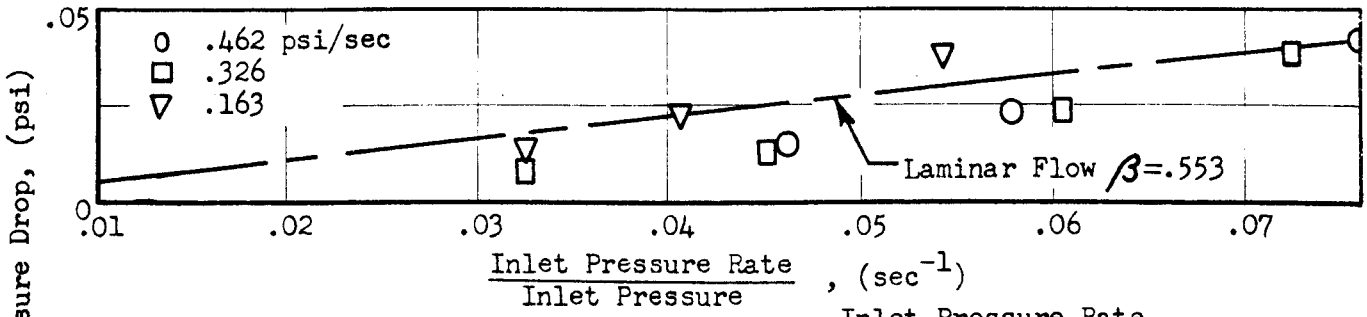

Figure 27 Frictional Pressure Drop vs. $\frac{\text{Inlet Pressure Rate}}{\text{Inlet Pressure}}$ for System No. 5 Pilot's Panel
Volume = 77 cu. in. Pitot Tube B

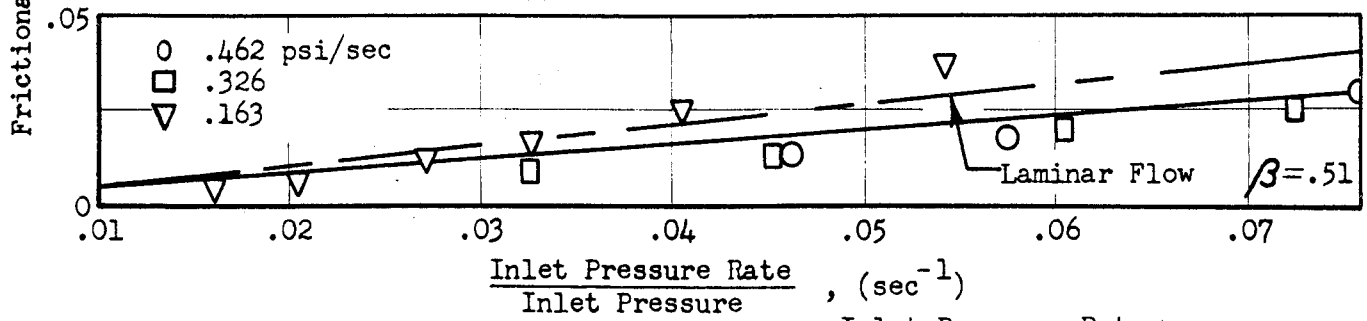

Figure 28 Frictional Pressure Drop vs. $\frac{\text{Inlet Pressure Rate}}{\text{Inlet Pressure}}$ for System No. 5 CADC Pressure Transducer
Volume = 17 cu. in. Pitot Tube B

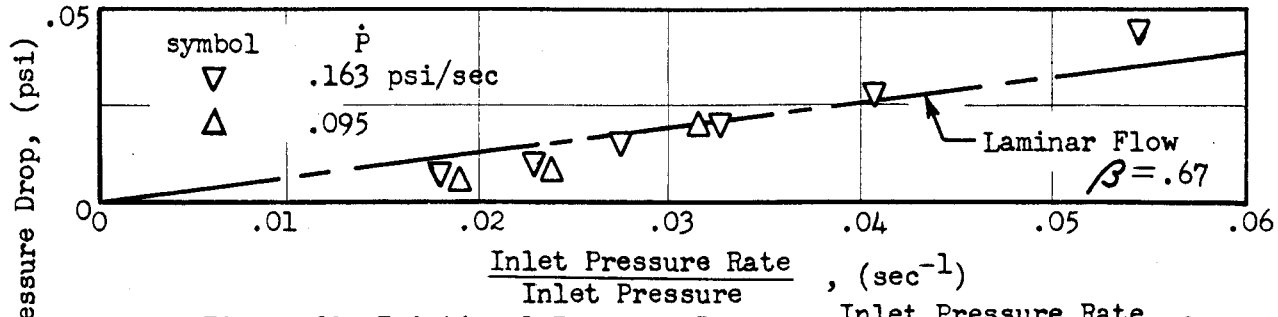

Figure 29 Frictional Pressure Drop vs. $\frac{\text{Inlet Pressure Rate}}{\text{Inlet Pressure}}$ for System No. 5 Pilot's Panel
Volume = 77 cu. in. Pitot Tube C

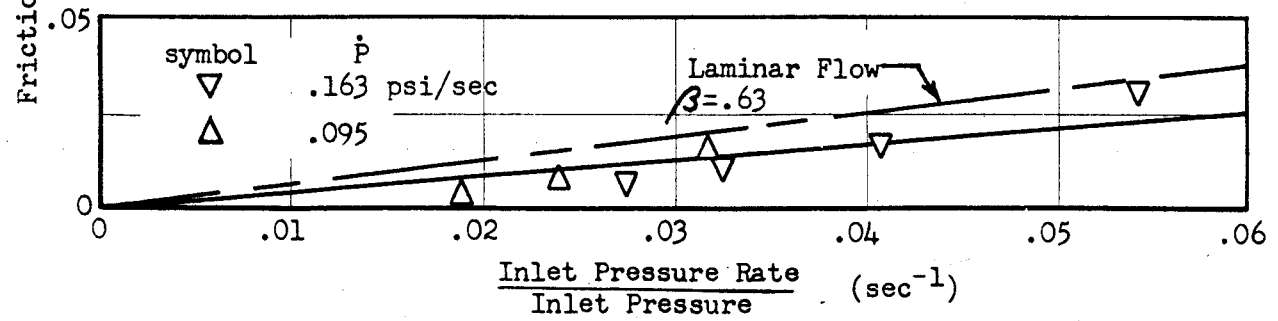

Figure 30 Frictional Pressure Drop vs. $\frac{\text{Inlet Pressure Rate}}{\text{Inlet Pressure}}$ for System No. 5 CADC Pressure Transducer
Volume = 17 cu. in. Pitot Tube C

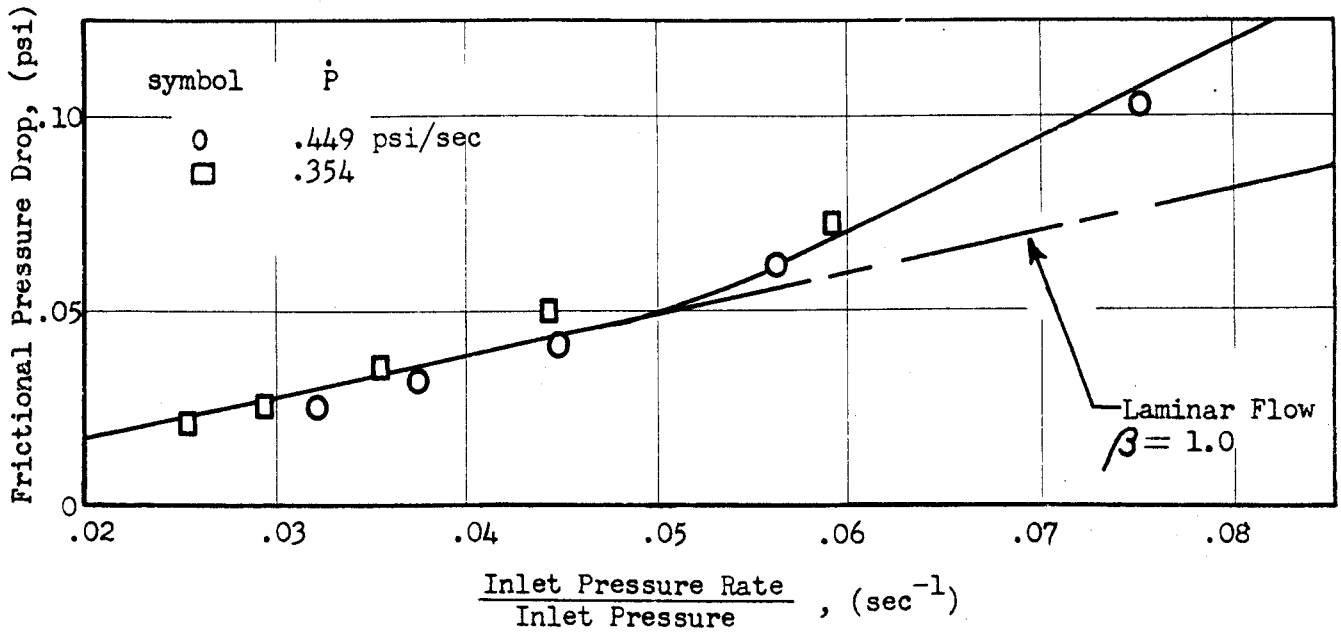

Figure 31 Frictional Pressure Drop vs. $\frac{\text{Inlet Pressure Rate}}{\text{Inlet Pressure}}$ for
System No. 5 Pilot's Panel
Volume = 77 cu. in. Pitot Tube D

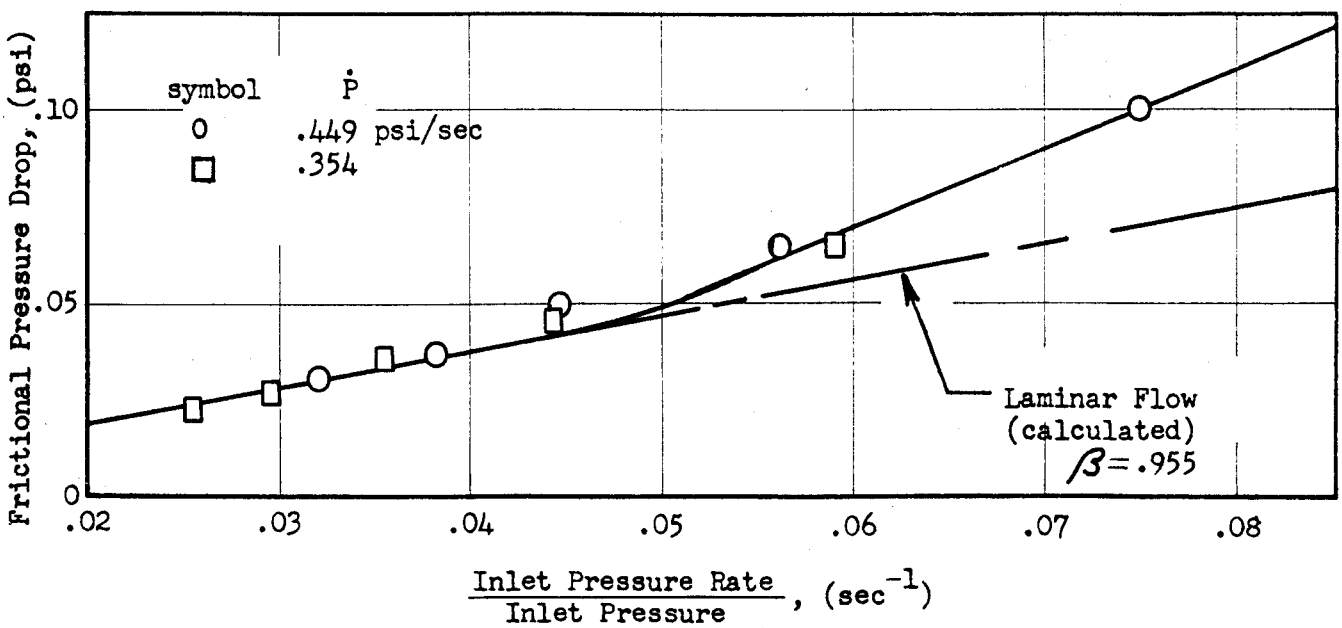

Figure 32 Frictional Pressure Drop vs. $\frac{\text{Inlet Pressure Rate}}{\text{Inlet Pressure}}$ for
System No. 5 CADC Pressure Transducer
Volume = 17 cu. in. Pitot Tube D

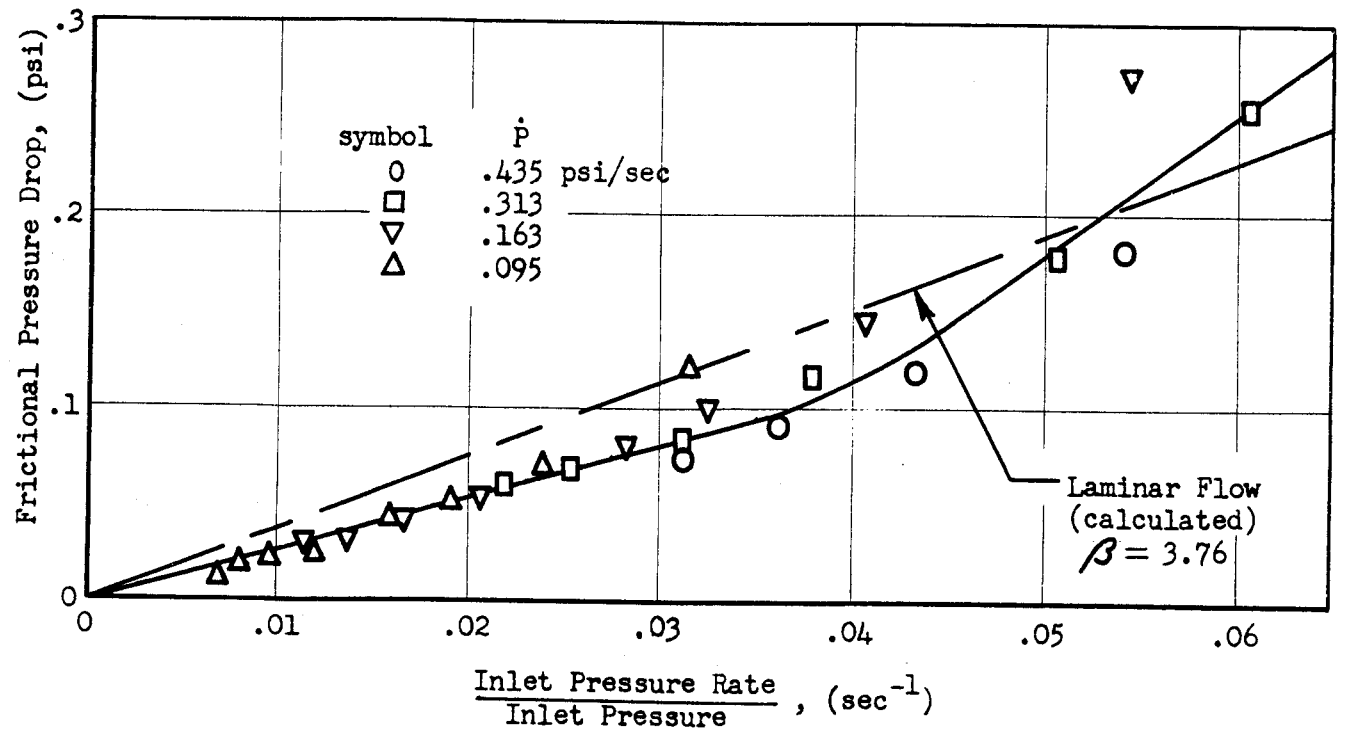

Figure 33 Frictional Pressure Drop vs. $\frac{\text{Inlet Pressure Rate}}{\text{Inlet Pressure}}$ for
System No. 6 Pilot's Panel
Volume = 77 cu. in. Pitot Tube A

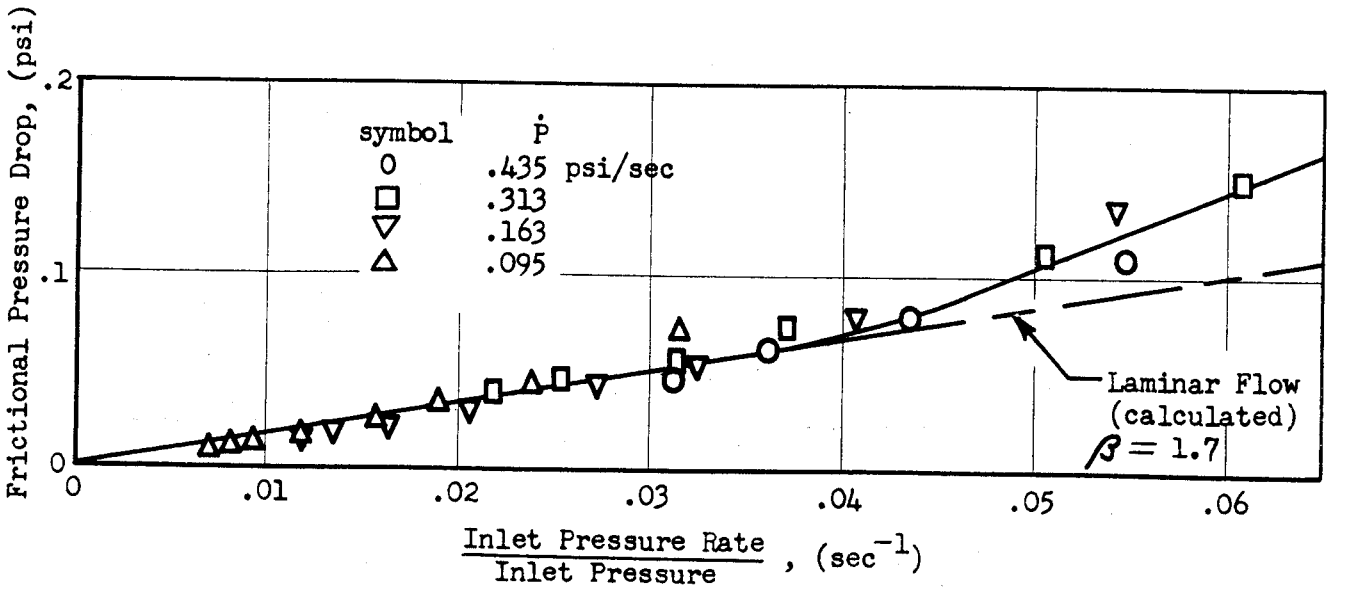

Figure 34 Frictional Pressure Drop vs. $\frac{\text{Inlet Pressure Rate}}{\text{Inlet Pressure}}$ for
System No. 6 CADC Pressure Transducer
Volume = 17 cu. in. Pitot Tube A

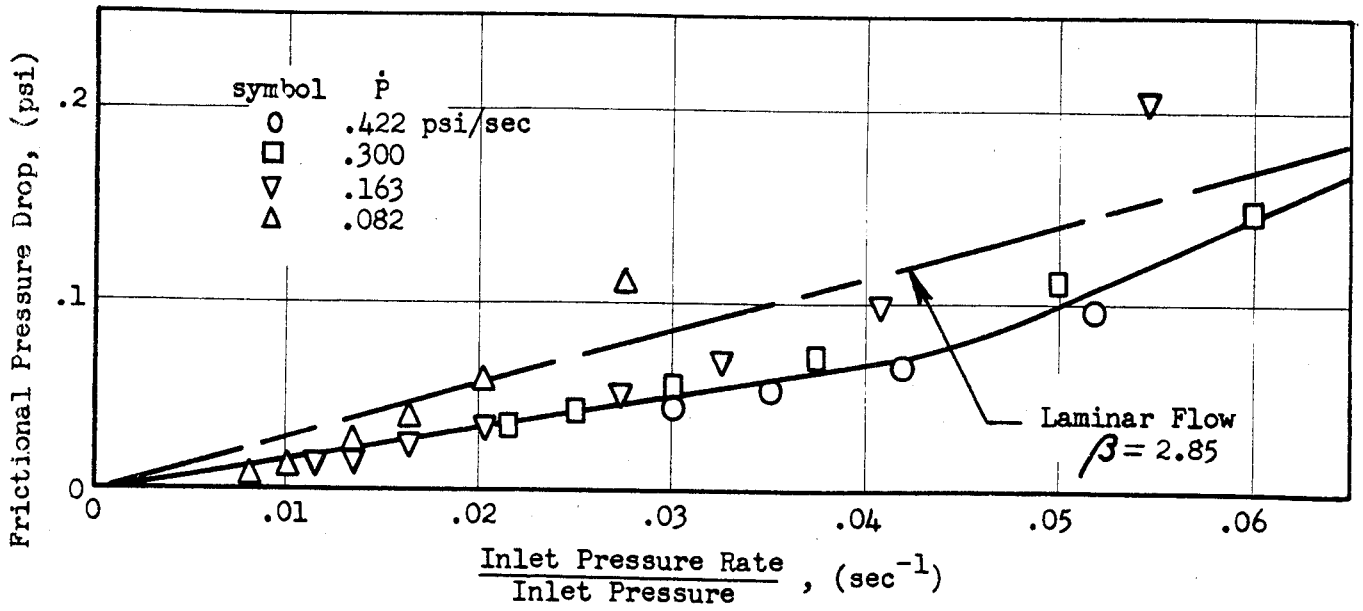

Figure 35 Frictional Pressure Drop vs. $\frac{\text{Inlet Pressure Rate}}{\text{Inlet Pressure}}$ for
System No. 6 Pilot's Panel
Volume = 77 cu. in. Pitot Tube B

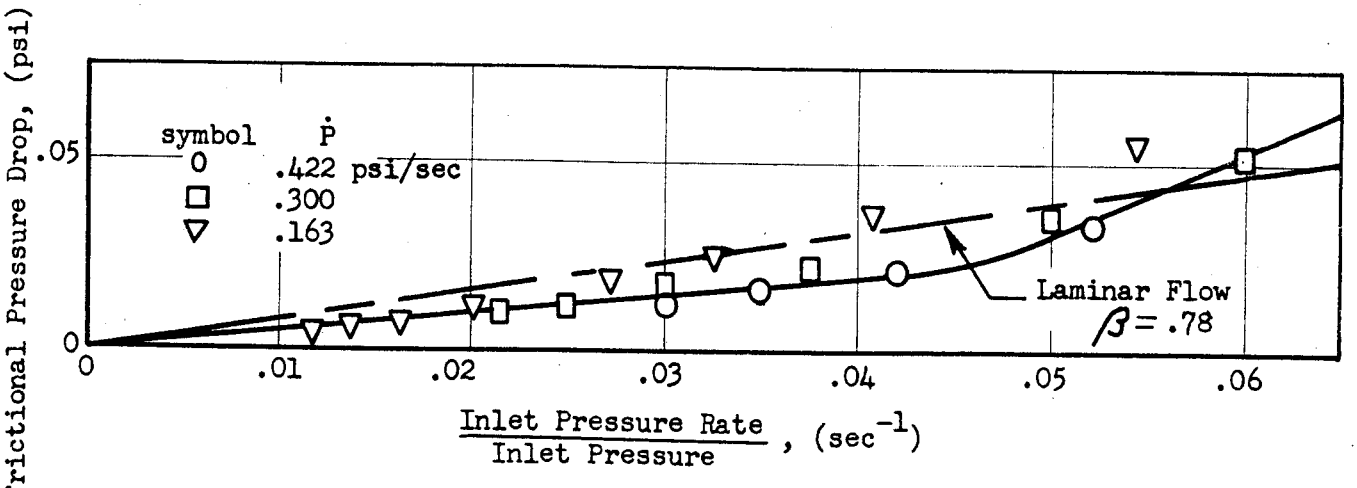

Figure 36 Frictional Pressure Drop vs. $\frac{\text{Inlet Pressure Rate}}{\text{Inlet Pressure}}$ for
System No. 6 CADC Pressure Transducer
Volume = 17 cu. in. Pitot Tube B

comparison of equations (2) and (8) of Article 3.2 which shows that the flow velocity is, for isothermal conditions,

$$v = \frac{1}{A}\left[A(\ell - X) + V\right]\frac{\dot{P}}{P} \tag{26}$$

Since $$Re \propto Dv$$

Then $$Re \propto \frac{1}{D}\left[A(\ell - X) + V\right]\frac{\dot{P}}{P} \tag{27}$$

Thus the Reynolds number is proportional to the total downstream volume, to $\dot{P}/P$, and inversely proportional to the internal diameter.

It is significant to note the influence of system geometry upon the critical value of $\dot{P}/P$, i.e., where transitional flow commences. As equation (26) indicates, the maximum velocity occurs when the downstream volume is the greatest and the flow area is the smallest. These conditions usually exist at or near the system inlet. It can be reasoned then that turbulence will probably begin at the pitot-static tube. Since the upper value of Reynolds number for laminar flow is nearly constant, equation (27) may be expressed as

$$\left[\frac{\dot{P}}{P}\right]_{cr} \propto \frac{D}{A\ell + V} \tag{28}$$

With the aid of this expression and Table 2 it is possible to explain the wide variation of $(\dot{P}/P)_{cr}$ for the arrangements tested. For example, consider two extreme cases: System 3 (Fig. 19) and System 4 (Figs. 21-24). Since the same pitot tube was used for both systems, the main tubing diameter may be utilized to compare these two systems with System 1. For systems 1 and 3 (using equation 28),

$$\frac{\left(\frac{\dot{P}}{P}\right)_{cr \text{ for No. } 3}}{\left(\frac{\dot{P}}{P}\right)_{cr \text{ for No. } 1}} = \frac{\frac{1}{4}}{\frac{1}{4}} \times \frac{120}{25} \approx 5$$

Since $(\dot{P}/P)_{cr}$ for No. 1 = .025, then $(\dot{P}/P)_{cr}$ for No. 3 = .125 which is off-scale as indicated in Table 2. For systems 1 and 4,

$$\frac{\left(\frac{\dot{P}}{P}\right)_{cr \text{ for No. } 4}}{\left(\frac{\dot{P}}{P}\right)_{cr \text{ for No. } 1}} = \frac{\frac{3}{8}}{\frac{1}{4}} \times \frac{120}{235} \approx \frac{3}{4}$$

In this case $(\dot{P}/P)_{cr}$ for No. 4 = 3/4 (.025) = .018, which is in agreement with Table 2 and Figures 21-24.

The lag contribution of various pitot tube designs is shown in Table 3. It

TABLE 2

MAJOR DIMENSIONS OF SYSTEMS TESTED

System No.	Figure No.	D_{eq} for Pitot Tube (in.)	OD of Main Tubing Line (in.)	Total Volume Downstream of Pitot Tube (cu. in.)	Approximate Value of $(\dot{P}/P)_{cr}$ from Graphs (sec^{-1})
1	12, 13 14	.101	1/4	120	.025
2	15, 16 17	.101	3/8	155	.025
3	18, 20	.101	1/4	102	.025
	19	.101	1/4	25	off-scale
4	21, 22, 23, 24	.101	3/8	235	.015
5	25, 26	.101	3/8	122	.040
	27, 28	.225	3/8	122	off-scale
	29, 30	.180	3/8	122	off-scale
	31, 32	.118	3/8	122	.050
6	33, 34	.101	1/4	114	.040
	35, 36	.225	1/4	114	.040

TABLE 3

LAG CONTRIBUTION OF VARIOUS PITOT TUBES ON SYSTEM NO. 5
(Based on calculated data)

Pitot Tube	Panel Lag Constant (λ_o, sec)	Lag Contribution of Tube (sec)	Percentage of Total Lag Due to Tube %
A	.104	.071	68.5
B	.0375	.008	21.3
C	.0457	.017	37.2
D	.068	.037	54.4

is clearly evident from this tabulation that Tubes A and D unduly penalize a high response system such as No. 5. Thus, the full lag reduction potential of 3/8 OD tubing cannot be achieved with pitot tubes similar to A and D.

Since fittings were not considered in the calculations, it is seen from the graphs that their contribution to lag in the laminar range is negligible. It is suspected, however, that they have a greater influence when the flow becomes transitional or partially turbulent. The same is also true for tubing bends. Newman (ref. 8) found that, during laminar flow, curvature effects in a length ℓ with a bend diameter δ are small when

$$\frac{V_d + \frac{A\ell}{2}}{D\mu} \dot{\rho} \left(\frac{D}{\delta}\right)^{1/2} < 11$$

In the WADC tests the largest possible bend radii (much larger than the limiting case) were utilized.

SECTION V

CONCLUSIONS AND RECOMMENDATIONS

In relation to the previously-stated objectives of the experimental phase and the entire program, the conclusions resulting from this investigation are summarized below:

1. The theoretical pressure lag analysis discussed herein is satisfactory for purposes of system comparison and is adequate for actual lag determination for the case of laminar flow.

2. Pitot-static tube designs similar to A and D (Fig. 10) are unsatisfactory because of their large lag contribution when connected to a system of typical internal volume. Tube designs B and C are considered satisfactory.

3. In general, the single-source system incorporating 3/8 OD tubing possesses the most desirable lag reduction characteristics of the arrangements considered.

On the basis of these conclusions it is recommended that, unless specialized requirements demand otherwise, the static pressure systems of high performance aircraft be composed of 3/8 in. OD (.035 wall) tubing in single-source arrangements similar to Systems 2, 4, and 5 of Figure 9. To achieve the full response capability of the large tubing it is further recommended that the limiting equivalent circular diameter of annular chambers in pitot-static tubes be a minimum of 3/16 inch. The minimum size for circular static pressure tubes inside the pitot-static tube should be 1/4 inch.

It is also suggested that applicable USAF static pressure system installation specifications be modified to require the following:

(1) Submission by the airframe contractor to WADC of lag analyses (theoretical and/or experimental) of system arrangements proposed during the design phase.

(2) An experimental verification of the response characteristics of the static pressure system utilized in the production air vehicle.

Since the WADC investigation was intended primarily to provide guides for the designer in choosing a high response system, no effort was made to establish techniques for determining or predicting lag errors during actual flight conditions. These subjects have been well covered by other investigators (refs. 4,5, and 13). There are two topics, however which, because of their relation to systems discussed herein, should receive further attention. They are:

(1) Effect of extremely high altitudes(above 80,000 feet) upon lag error. At these heights the mean free path of the air molecules becomes comparatively large and a phenomena known as slip flow occurs.

(2) Influence of low damping levels which may be present in high response systems. This could result in severe pressure oscillations at low altitudes under unsteady inlet conditions.

REFERENCES

1. Charnley, W.J., A Note on a Method of Correcting for Lag in Aircraft Pitot-Static Systems, R & M No. 2352, Royal Aeronautical Establishment Report No. Aero 2516, 1950.

2. Goroshchanko, L., Instrument Indication Delays, Air Fleet Herald, USSR, No. 3, 1955. pp. 45-52. (Translation by USAF Air Technical Intelligence Center, Wright-Patterson AFB, Ohio.)

3. Grupsmith, N., Lag in Altimeter Indication During High Speed Dives, Report No. NAES-INSTR-24-26, Aeronautical Instruments Laboratory, Bureau of Aeronautics, USN, August 1946.

4. Head, R.M., Lag Determination of Altimeter Systems, Journal of Aeronautical Sciences, Vol. 12, No. 1, January 1945.

5. Huston, W.B., Accuracy of Airspeed Measurements and Flight Calibration Procedures, NACA Report No. 919, 1948.

6. Iberall, A.S., Attenuation of Oscillatory Pressures in Instrument Lines, National Bureau of Standards Research Paper RP 2115, July 1950.

7. Kendal, J.M., Time Lags Due to Compressible Poiseuille Flow Resistance in Pressure Measuring Systems, Naval Ordinance Laboratory Memorandum No. 10677, May 1950.

8. Newman, B.G., Lag in Airborne Pressure Measuring Systems, National Aeronautical Establishment, Canada, Report No. LR-100, April 1954.

9. Perry, J.A., Critical Flow Through Sharp-Edged Orifices, Transactions of the ASME, October 1949.

10. Reid, R.J., and Campbell, B.J., Pneumatic Response Characteristics of Nose-Boom Pitot Systems Using Ramp Function Inputs, Convair Report 56-234 Addendum I, July 1956.

11. Shapiro, A.H., Dynamics and Thermodynamics of Compressible Fluid Flow, Volume I, Ronald Press Co., New York, N.Y., 1953.

12. Sinclair, A.R., and Robins, A.W., A method for the Determination of the Time Lag in Pressure Measuring Systems Incorporating Capillaries, NACA Technical Note 2793, September 1952.

13. Smith, K.W., Pressure Lag in Pipes With Special to Aircraft Speed and Height Measurements, Royal Aeronautical Establishment Report No. Aero 2507, Nov. 1954.

14. Vaughn, H., The Response Characteristics of Airplane and Missile Pressure Measuring Systems, Aeronautical Engineering Review, November 1955.

15. Wildhack, W.A., Pressure Drop in Tubing in Aircraft Instrument Installations, NACA Technical Note 593, February 1937.

APPENDIX I

DERIVATION SUMMARY 1

The general vector form of the Navier-Stokes equation is

$$\frac{d\upsilon}{dt} = \frac{\mu}{\rho}\nabla^2\upsilon - \frac{1}{3\rho}\nabla(\nabla\cdot\upsilon) - \frac{1}{\rho}\nabla P \tag{1}$$

For one-dimensional, steady flow, equation (1) reduces to

$$\frac{r}{\mu}\frac{\partial P}{\partial X} = \frac{\partial}{\partial r}\left(r\frac{\partial \upsilon}{\partial r}\right) \tag{2}$$

Integrating equation (2) twice yields the following expression:

$$\upsilon = \frac{1}{4\mu}\frac{\partial P}{\partial X}r^2 + C_1 \ln r + C_2 \tag{3}$$

The two integration constants are determined from the boundary conditions which are (from the sketch at right):

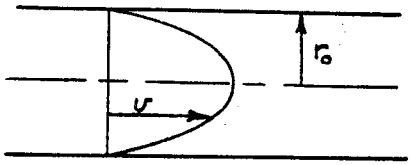

$$\upsilon = 0 \text{ when } r = r_o$$

$$\frac{\partial \upsilon}{\partial r} = 0 \text{ when } r = 0$$

Then

$$\left.\begin{aligned} C_1 &= 0 \\ C_2 &= -\frac{1}{4\mu}\frac{\partial P}{\partial X}r_o^2 \end{aligned}\right\} \tag{4}$$

Substituting equation (4) into (3) yields

$$\upsilon = \frac{1}{4\mu}\frac{\partial P}{\partial X}\left(r^2 - r_o^2\right) \tag{5}$$

If $\bar{\upsilon}$ is the average velocity, then

$$A\bar{\upsilon} = 2\pi\int_0^{r_o}\upsilon\, r\, dr \tag{6}$$

Substituting equation (5) into (6), integrating, and simplifying gives

$$\frac{\partial P}{\partial X} = -\frac{8\mu\bar{\upsilon}}{r_o^2} = -\frac{32\mu\bar{\upsilon}}{D_o^2}$$

DERIVATION SUMMARY 2

Equation (20), Article 3.3, is repeated below for reference

$$\Delta P_f\Big]_{\ell} = \Delta P_f\Big]_{K} + \Delta P_f\Big]_{\ell-K} \tag{20}$$

Applying equation (11) (Article 3.2) to each term of the above expression yields

$$\frac{128\mu\ell}{\pi D^4}\left(V+\frac{A\ell}{2}\right) = \frac{128\mu}{\pi D^4}\left[(\ell-K)\left\{AK+V+\frac{A(\ell-K)}{2}\right\}+K\left(V+\frac{AK}{2}\right)\right] \tag{1}$$

Expanding and simplifying this equation gives

$$\ell\left(V+\frac{A\ell}{2}\right)=\left[A\ell K+V\ell+\frac{A\ell^2}{2}-\frac{A\ell K}{2}-AK^2-KV-\frac{A\ell K}{2}+\frac{AK^2}{2}+KV+\frac{AK^2}{2}\right] \tag{2}$$

It is seen that equation (2) reduces to the identity

$$\ell\left(V+\frac{A\ell}{2}\right)\equiv V\ell+\frac{A\ell^2}{2} \tag{3}$$

This indicates that the term V in equation (11) can represent the <u>total</u> volume downstream from the tubing length under consideration.

DERIVATION SUMMARY 3

The boundary conditions for laminar flow in an annular chamber are:

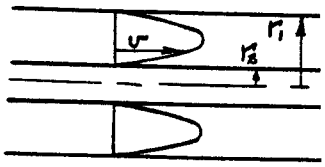

$$\left.\begin{aligned} v = 0 \quad &\text{when} \quad r = r_1 \\ v = 0 \quad &\text{when} \quad r = r_2 \end{aligned}\right\} \qquad (1)$$

Substituting equation (1) into equation (3) of Derivation Summary 1 gives the two constants of integration.

$$C_1 = -\frac{1}{4\mu}\frac{\partial P}{\partial X}\left[\frac{r_1^2 - r_2^2}{\ln \frac{r_1}{r_2}}\right]$$

$$C_2 = -\frac{1}{4\mu}\frac{\partial P}{\partial X}\left[\frac{r_1^2 \ln r_2 - r_2^2 \ln r_1}{\ln \frac{r_1}{r_2}}\right]$$

The velocity equation is then

$$v = \frac{1}{4\mu}\frac{\partial P}{\partial X}\left[r^2 - \left(\frac{r_1^2 - r_2^2}{\ln \frac{r_1}{r_2}}\right)\ln r \; - \; \frac{r_1^2 \ln r_2 - r_2^2 \ln r_1}{\ln \frac{r_1}{r_2}}\right] \qquad (2)$$

If $\bar{v}$ is the average velocity, then

$$A\bar{v} = 2\pi \int_{r_2}^{r_1} v\, r\, dr \qquad (3)$$

If equation (2) is inserted into equation (3) and the resulting expression simplified, the result is

$$\frac{\partial P}{\partial X} = -\frac{8\mu\bar{v}}{r_1^2 + r_2^2 - \frac{r_1^2 - r_2^2}{\ln \frac{r_1}{r_2}}}$$

or

$$\frac{\partial P}{\partial X} = -\frac{32\mu\bar{v}}{D_1^2 + D_2 - \frac{D_1^2 - D_2^2}{\ln \frac{D_1}{D_2}}}$$

APPENDIX II

Sample Lag Calculations

For 1/4 OD X .035 tubing

$$A = .785 \times .18^2 = .0254 \text{ in}^2$$

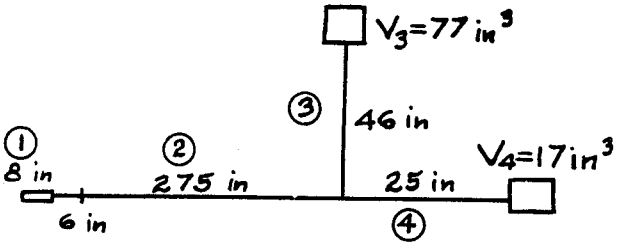

$$B = \frac{128 \times 3.71 \times 10^{-7} \text{ slugs/ft.-sec.}}{\pi \times (.18 \text{ in})^4 \times 2116 \text{ psf}}$$

$$= 6.88 \times 10^{-6} \text{ sec/in}^4$$

For the annular chamber (D_{eq} = .19 and 8 long)

$$\lambda_o = 6.88 \times 10^{-6} \text{ sec/in}^4 \times \left(\frac{.18}{.19}\right)^4 \times 8 \text{ in} \times V_d = 4.55 \times 10^{-5} V_d \text{ sec/in}^3$$

For static pressure ports (D = .080 and 3/16 long)

$$\lambda_o = 6.88 \times 10^{-6} \text{ sec/in}^4 \times \left(\frac{.18}{.08}\right)^4 \times \frac{3}{16} \text{ in} \times \frac{V_d}{2} = 1.66 \times 10^{-5} V_d \text{ sec/in}^3$$

For annular chamber and ports

$$\lambda_{o1} = (4.55 + 1.66) \times 10^{-5} V_d = 6.21 \times 10^{-5} V_d \text{ sec/in}^3$$

Now, from sketch at top of page,

$$\lambda_{o4} = 6.88 \times 10^{-6} \times 25 \text{ in} \times (17 \text{ in}^3 + 12.5 \times .0254 \text{ in}^3) = .00298 \text{ sec}$$

$$\lambda_{o3} = 6.88 \times 10^{-6} \times 46 \times (77 + 23 \times .0254) = .0246 \text{ sec}$$

$$\lambda_{o2} = 6.88 \times 10^{-6} \times 281 \times (94 + 210 \times .0254) = .192 \text{ sec}$$

$$\lambda_{o1} = 6.21 \times 10^{-5} \times (94 + 358 \times .0254) = .0063 \text{ sec}$$

$$\left(\frac{\ell}{a_o}\right)_{V_3} = \frac{335 \text{ in}}{12{,}000 \text{ in/sec}} = .0279 \text{ sec}$$

$$\left(\frac{\ell}{a_o}\right)_{V_4} = \frac{314 \text{ in}}{12{,}000 \text{ in/sec}} = .0262 \text{ sec}$$

Then

$$\left[\lambda_o + \frac{\ell}{a_o}\right]_{V_3} = \lambda_{o1} + \lambda_{o2} + \lambda_{o3} + \frac{\ell}{a_o} = .251 \text{ sec}$$

$$\left[\lambda_o + \frac{\ell}{a_o}\right]_{V_4} = \lambda_{o1} + \lambda_{o2} + \lambda_{o4} + \frac{\ell}{a_o} = .227 \text{ sec}$$